BAMS Article

A Historical Overview on the Science of Derechos

Part II: Parent Storm Structure, Environmental Conditions, and History of Numerical Forecasts

Brian Joseph Squitieri, Andrew R. Wade, and Israel L. Jirak

KEYWORDS:
Convective storms/systems;
Mesoscale systems;
Derecho;
Forecasting;
Numerical weather prediction/forecasting

ABSTRACT: Over the course of the century, much research has been done to understand how derechos form, what environments support derecho development, and how forecasts of derechos can be improved. Following the definition, climatology, and societal impacts of derechos in Part I of this manuscript, Part II offers a thorough review on the parent MCS structures that produce derechos, which synoptic setups support derecho-producing MCSs, and the successes and failures of forecasting derechos. This manuscript reviews the 3D structure of MCSs that support derecho development, as well as both the strongly and weakly forced synoptic environments where derechos frequently occur. In addition, successes and failures common among most derecho numerical forecast studies are discussed to suggest where the greatest improvements in derecho forecasting may be made.

https://doi.org/10.1175/BAMS-D-22-0278.1
Corresponding author: Brian Joseph Squitieri, brian.squitieri@noaa.gov
In final form 10 June 2023

AFFILIATIONS: Squitieri, Wade, and Jirak—Storm Prediction Center, NOAA/National Weather Service/ National Centers for Environmental Prediction, Norman, Oklahoma

A review on derecho-supporting MCS structure and dynamics

The understanding of the physical mechanisms responsible for derecho production, particularly progressive derechos, stems from earlier studies of the vertical convective circulations that characterize linear derecho-producing mesoscale convective system (DMCS) structures. Beyond the squall line studies of Hamilton et al. (1945), Newton (1950), Tepper (1950), and Fujita (1955), numerous studies in the last 50 years have focused on MCS internal dynamics (Houze 2018) to understand why MCSs sustain themselves for long periods of time and support long-tracked derecho wind-damage swaths. Ascending front-to-rear flow from the MCS leading line to the trailing precipitation region supports the rearward transportation of rainwater, snow, and ice pellets, which melt and evaporate as they descend behind the main thunderstorm line (Ogura and Chen 1977; Rutledge and Houze 1987; Biggerstaff and Houze 1991; Zhang and Cho 1992; Sun et al. 1993; Gallus and Johnson 1995a,b; Tao et al. 1995; Braun and Houze 1995, 1996; Yang and Houze 1996). This ice melting and rainfall evaporation results in the development of a cold pool (Fujita 1959; Bryan and Parker 2010; Peters and Hohenegger 2017), consisting of colder, negatively buoyant air behind the MCS gust front (Fig. 1). The cold pool is highly influential on DMCS intensity, forward propagation speed, direction, and longevity (Corfidi 2003; Bentley and

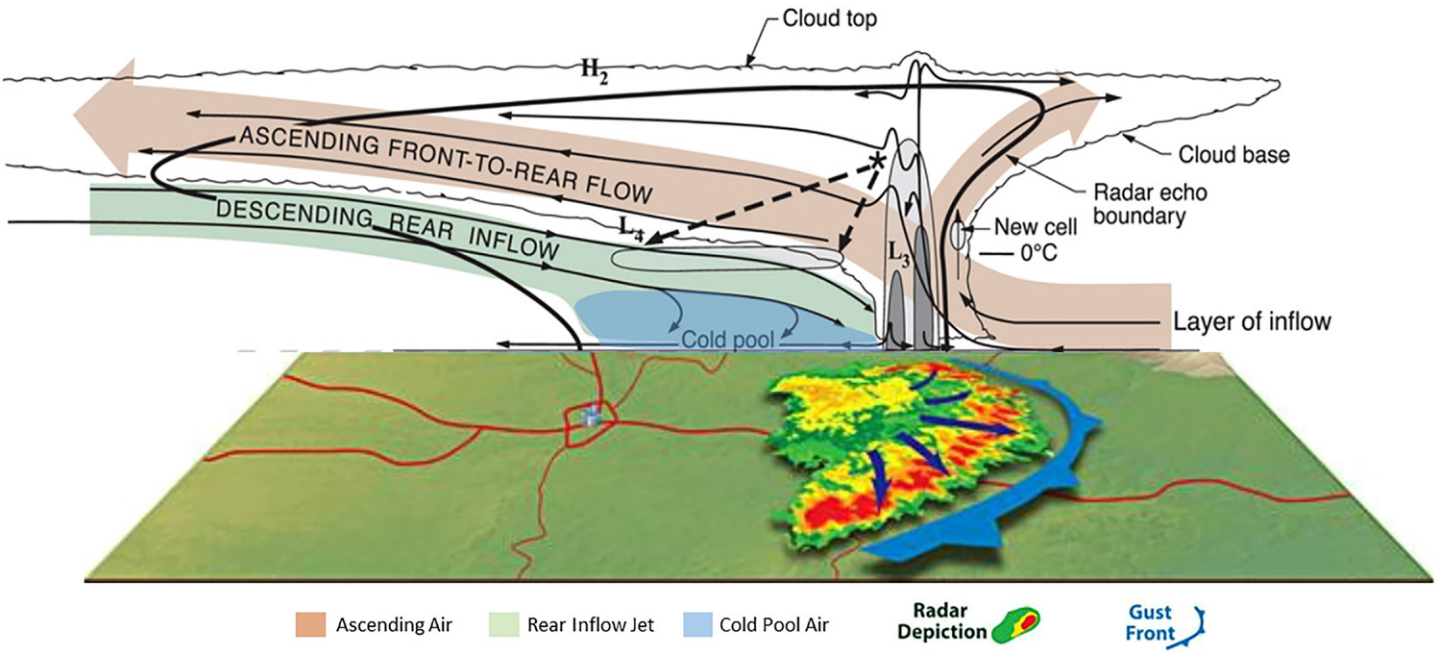

Fig. 1. Conceptual model of the kinematic, microphysical, and radar echo structure of a convective line with trailing precipitation viewed in a vertical cross section oriented perpendicular to the convective line (and generally parallel to its motion). Medium and dark shading indicate intermediate and strong radar reflectivities. Planar map depicts MCS appearance via composite reflectivity, with arrows depicting forward motion and a gust front preceding the main band of convective precipitation. [Originally from Houze et al. (1989, Fig. 1); adapted and augmented from Houze (2018, Fig. 17); planar map plot developed by Dennis Cain, National Weather Service (Southern Region), and modified by Stephen Corfidi, Storm Prediction Center.]

Logsdon 2016; Campbell et al. 2017) and is crucial for supporting damaging surface winds in weakly forced environments (Evans and Doswell 2001).

As the cold pool advances into warmer, buoyant air, a horizontal buoyancy gradient develops, leading to the development of a low-level horizontal circulation along the gust front, supporting MCS forward motion (Fig. 1). In environments of relatively weak low-level shear, the cold pool tends to undercut thunderstorm updrafts, shortening their lifespan (Fig. 2a). In MCS cases with relatively stronger low-level shear, the opposing horizontal circulation associated with the low-level shear may counter the cold-pool horizontal circulation, producing deeper lift along the cold pool's leading edge. The resulting enhanced low-level lift aids in air parcel ascent to the level of free convection, promoting new cellular development along the MCS leading line (Fig. 2b), effectively sustaining the MCS (Wilhelmson and Chen 1982; Droegemeier and Wilhelmson 1987; Xue 2002; Weisman and Rotunno 2004). Weisman (1992, 1993) found that the most intense and longest-lived simulated MCSs (i.e., those that support derechos), including bow echoes (Przybylinski 1995; Weisman 2001), thrived when cold-pool forward speed (C) was noticeably stronger than the magnitude of vertical wind shear (Δu) in the lowest 2.5 km above ground level (AGL), but with Δu strong enough to keep the cold pool from completely undercutting the bow echo leading line. With $C > \Delta u$, leading-line convection is forced to tilt upshear, sustaining the front-to-rear flow (Fig. 3), and augmenting the cold pool with continuous latent cooling from the rearward transport of additional melting ice and evaporating rainwater. Cold pools associated with DMCSs tend to be much colder and more expansive (thus more intense) over longer distances compared to cold pools associated with other MCSs (as was the case on 29 June 2012; Fig. 4), often supporting derecho wind swaths (Fovell and Ogura 1989; Evans and Doswell 2001; Coniglio and Stensrud 2001; Weisman et al. 2023).

The MCS cold-pool circulation overcoming low-level shear also results in the development of the rear-inflow jet (RIJ) after the MCS updrafts tilt upshear (Fig. 3c) (Lafore and Moncrieff 1989; Weisman 1992, 1993; Weisman and Rotunno 2004). The RIJ surges toward the MCS leading line from the trailing precipitation region while also descending in altitude (Fig. 1), supporting not only longer-lived MCSs (Charba 1974), but intense events capable of producing derecho wind swaths (Price and Murphy 2002; López 2007; Dunn and Best 2011; Coniglio et al. 2012; Bentley and Logsdon 2016; Mathias et al. 2017; Taszarek et al. 2019, among others). RIJs form when the front-to-rear ascending flow (Figs. 1 and 3c) in the upshear-tilted

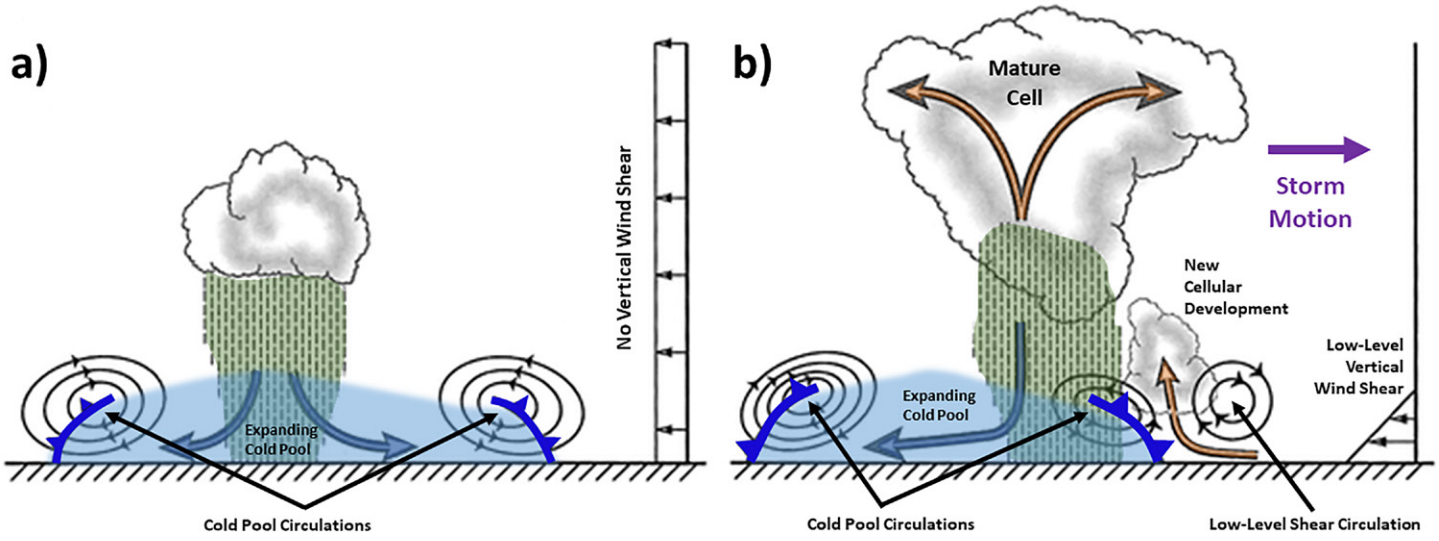

Fig. 2. (a) Cold pool spreads away from a decaying convective cell in an environment with no vertical wind shear. (b) Low-level vertical wind shear balances the cold-pool circulation on the downshear side, enhancing the ability to regenerate convective cells through deeper lifting. [Adapted and subjectively augmented from Weisman and Rotunno (2004, Fig. 1).]

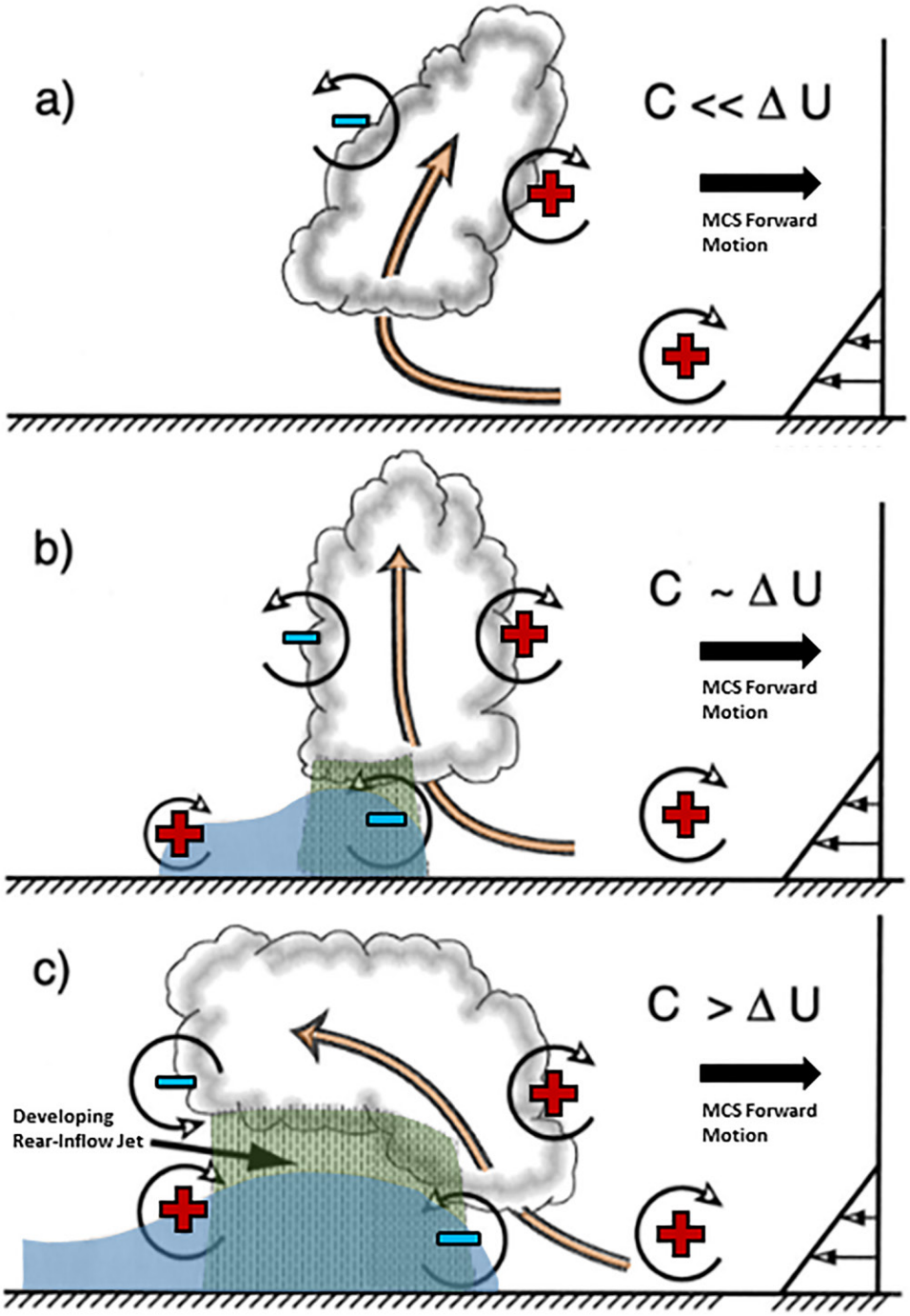

Fig. 3. Three stages in the evolution of an MCS. (a) An initial updraft leans downshear in response to the ambient vertical wind shear, which is shown on the right. (b) The circulation generated by the storm-induced cold pool balances the ambient shear, and the system becomes upright. (c) The cold-pool circulation overwhelms the ambient shear and the system tilts upshear, producing a rear-inflow jet. The updraft current is denoted by the thick, double-lined, orange-filled flow vector, and the rear-inflow current in (c) is denoted by the thick solid vector. The green shading denotes rainfall and the blue shading represents the surface cold pool. The thin circular arrows depict the most significant sources of horizontal vorticity, which result in the circulations either associated with the ambient shear or generated within the convective system. The scalloped line denotes the outline of the cloud. Here, *C* represents the strength of the cold pool while Δ*u* represents the strength of the ambient low-level vertical wind shear. [Originally from Weisman (1992, Fig. 2), then augmented from Weisman and Rotunno (2004, Fig. 2).]

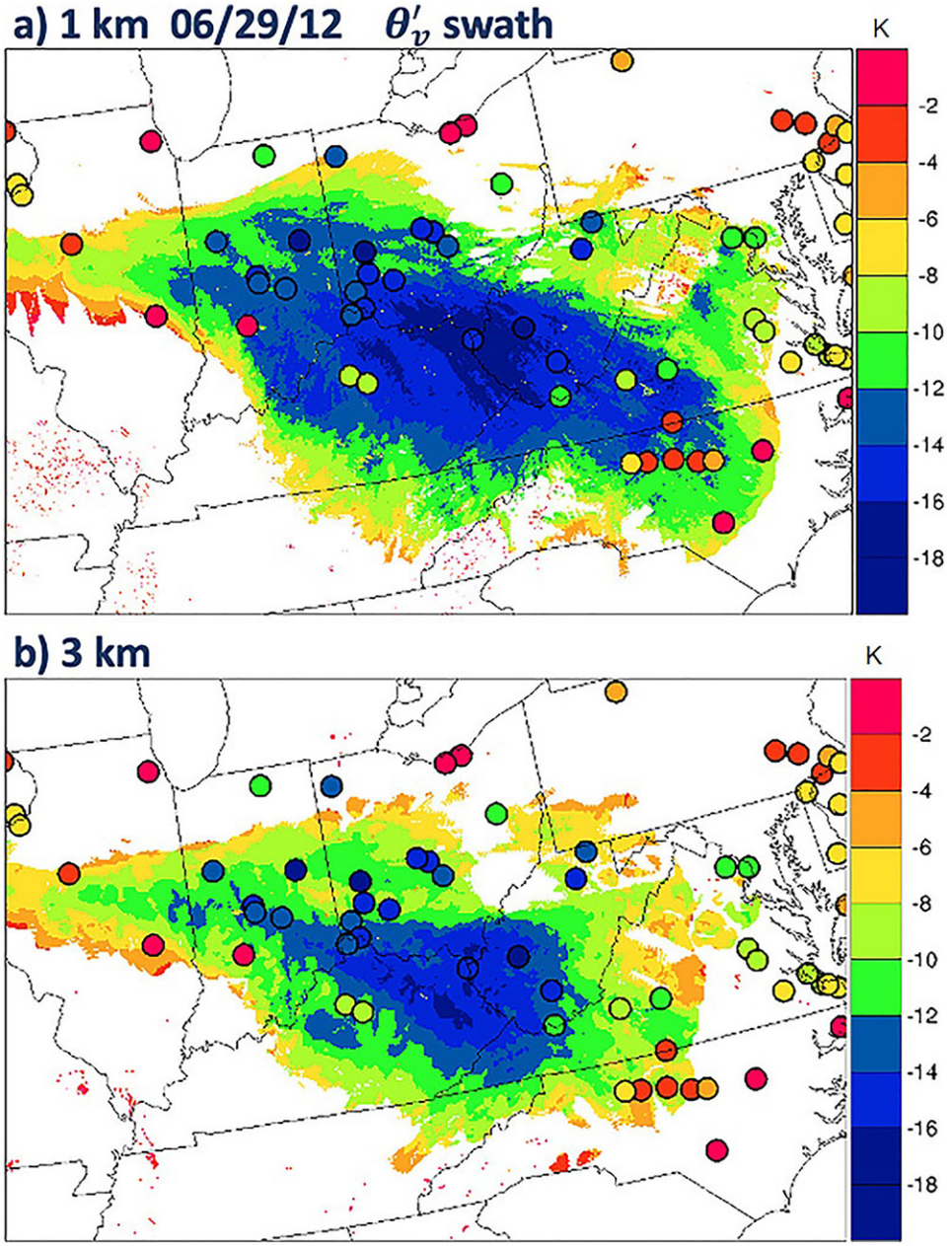

Fig. 4. Swaths of maximum surface perturbation virtual potential temperature $\theta'v$ (shading; K) for 29 Jun 2012 for the (a) 1 and (b) 3 km WRF-ARW simulations, which shows the cumulative intensity and expanse of the DMCS cold pool for much of its life cycle. Colored dots represent the equivalent maximum observed θ'_v for all available Automated Surface Observing Systems for this case. The negative values below −10 K (in cool colors) denotes where the cold pool was most intense. [Adapted from Weisman et al. (2023)].

thunderstorm updrafts transports buoyant air parcels upward and behind the MCS leading line, atop the stable cold pool, supporting the horizontal buoyancy gradient (Weisman 1992). Horizontal vorticity develops from this buoyancy gradient, resulting in opposing circulations between the cold pool and more unstable air aloft, which accelerates midlevel air parcels from the trailing precipitation region toward the MCS leading line (Fig. 3c). RIJs can be detected in real time using regional radar data when parent MCS forward motion is aligned with the radar beam (Fig. 5a). The RIJ becomes pronounced via strong inbound (outbound) velocities in low-level tilts of planar data as the MCS moves toward (away) from the radar site (Fig. 5b). Vertical slices of regional radar data would reveal intense velocities descending from the rear of the parent MCS to the leading line of more intense convection (Figs. 5c,d). Early detection of the RIJ in bow echo MCSs and DMCSs may lead to timely

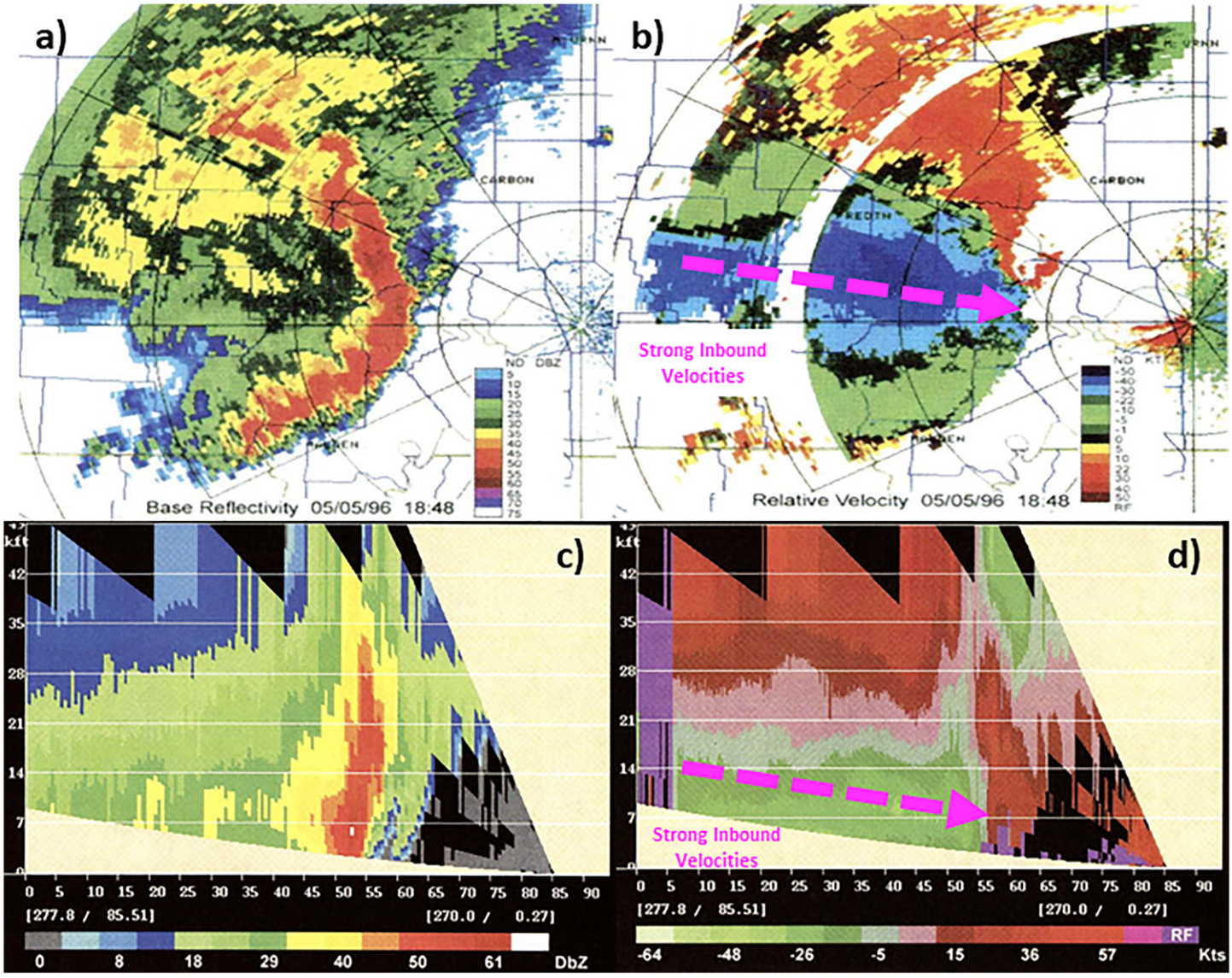

Fig. 5. (a) Base reflectivity and (b) relative velocity from the Paducah Kentucky (KPAH), WSR-88D at 1848 UTC 5 May 1996. Velocities are presented relative to a storm motion of 17 m s^{-1} from 280°. Vertical cross sections of (c) reflectivity and (d) storm-relative velocity at 1854 UTC for the KPAH bow echo, as also depicted in (a) and (b). The vertical cross sections are taken at a 277° heading from KPAH. Velocities are presented relative to a storm motion of 10 m s^{-1} from 277°. [The plots in (a) and (b) and in (c) and (d) are adapted from Figs. 14 and 15, respectively, of Weisman (2001).]

warnings that can convey the appropriate level of danger associated with a widespread severe thunderstorm wind event.

RIJs can also descend to near the surface over a broader area due to latent cooling when traversing the trailing precipitation region, where melting ice species and rainfall evaporation increases downward momentum transport (Zhang and Gao 1989; Biggerstaff and Houze 1991; Yang and Houze 1995; Braun and Houze 1997; James et al. 2006; McFarquhar et al. 2007; Grim et al. 2009). Mahoney and Lackmann (2011) found that drier RIJs, benefitting from relatively greater latent cooling, allowed for additional downward momentum transport, enhancing damaging wind potential in simulated bow echo MCSs (Fig. 6). The stronger surface winds in the drier simulations were present from the MCS leading line to the cold-pool region (leading and trailing wind maxima; Fig. 6b). In DMCS cases with dry, intense RIJs, prolonged exposure to severe winds may occur, as was the case for the 10 August 2020 derecho, where locales in eastern Iowa experienced 50+ kt (1 kt ≈ 0.51 m s^{-1}) winds for over 45 min (Bell et al. 2022).

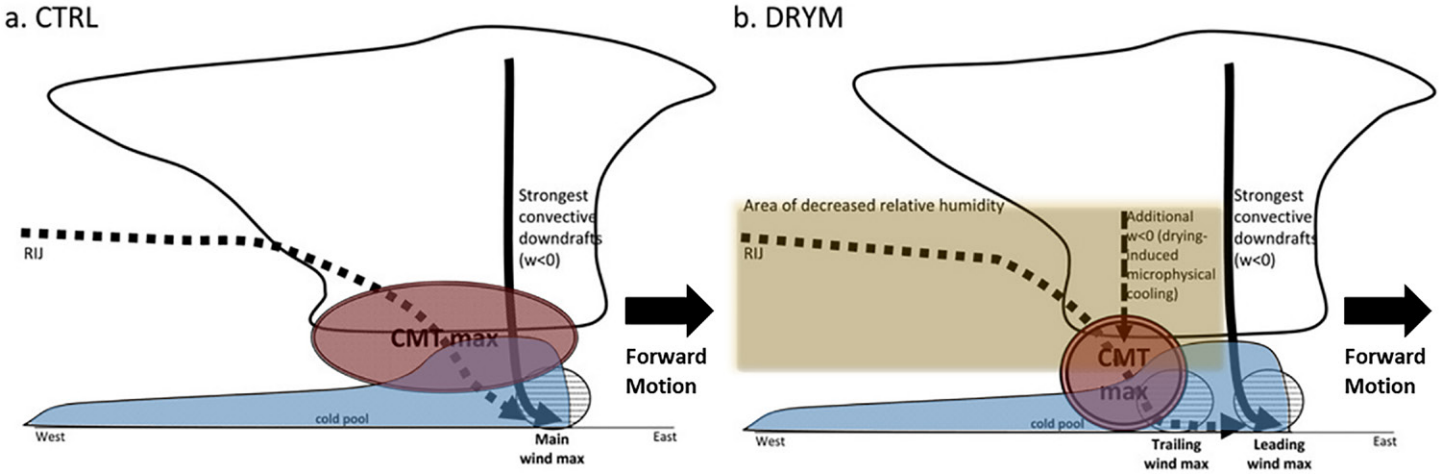

Fig. 6. Schematic of severe wind generation mechanisms in (a) the control (CTRL) simulation and (b) the dry RIJ (DRYM) simulation of an idealized MCS. Blue shading denotes the cold pool and red shading indicates where the greatest downward momentum transport occurs. Smaller hashed circles indicate where the most intense winds approached the surface. The yellow-shaded area in (b) denotes a drier airmass in the trailing precipitation region behind the MCS leading line. [Adapted from Mahoney and Lackmann (2011, Fig. 14).]

The development of a strong cold pool and RIJ may support mesovortex development and derecho occurrence. Fujita (1978) was among the first to attribute a system-scale line-end mesovortex with a destructive wind-producing MCS event (Fig. 7), with MCS mesovortices becoming a focus of study for DMCS events in subsequent decades.

System-scale line-end mesovortices often develop with bow echo DMCSs when primarily front-to-rear (Fig. 8a) or sometimes rear-to-front (Fig. 8b) flow along the MCS leading line tilts horizontal vorticity (associated with the low-level shear countering the cold pool), which is stretched at the midlevels along the ends of the DMCS line due to convergence from convective downdrafts (Weisman 1993; Weisman and Davis 1998). A pressure gradient force between the line-end vortices may enhance the RIJ and intensify the bow echo (Fig. 8c) (Weisman 1993; Wakimoto et al. 2006a; Grim et al. 2009), supporting derecho wind swaths. Through bow echo evolution, the southern line-end vortex weakens (Weisman and Davis 1998; Pandya et al. 2000) as the northern vortex dominates with assistance from the Coriolis force (Houze et al. 1989; Scott and Rutledge 1995; Wheatley and Trapp 2008), resulting in the classic cyclonic MCS structure often seen with intense bow echo DMCSs (Fujita 1978; Przybylinski 1995; Weisman 2001). A historic example of a system-scale line-end mesovortex influencing DMCS intensity would be the 8 May 2009 "super derecho," which produced extensive destructive winds across southern Missouri and Illinois, very near the track of the line-end vortex (Fig. 9).

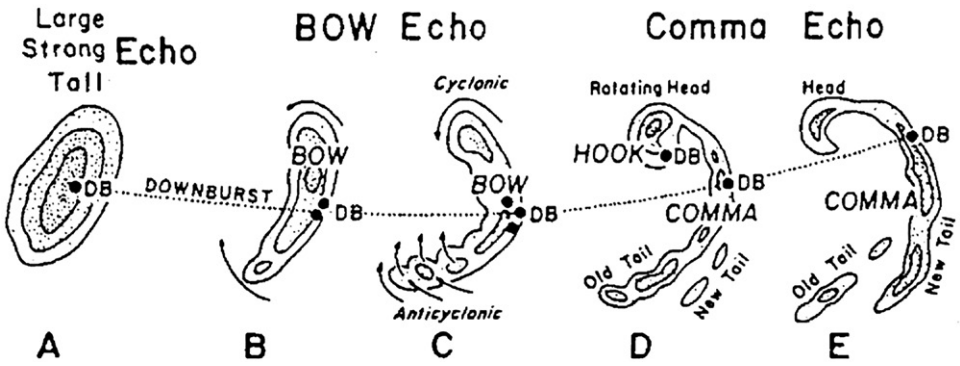

Fig. 7. A conceptual model of the bow echo MCS life cycle, with the development of a system-scale line-end mesovortex north of the bow in stages C–E. [From Fujita (1978, Fig. 5.2).]

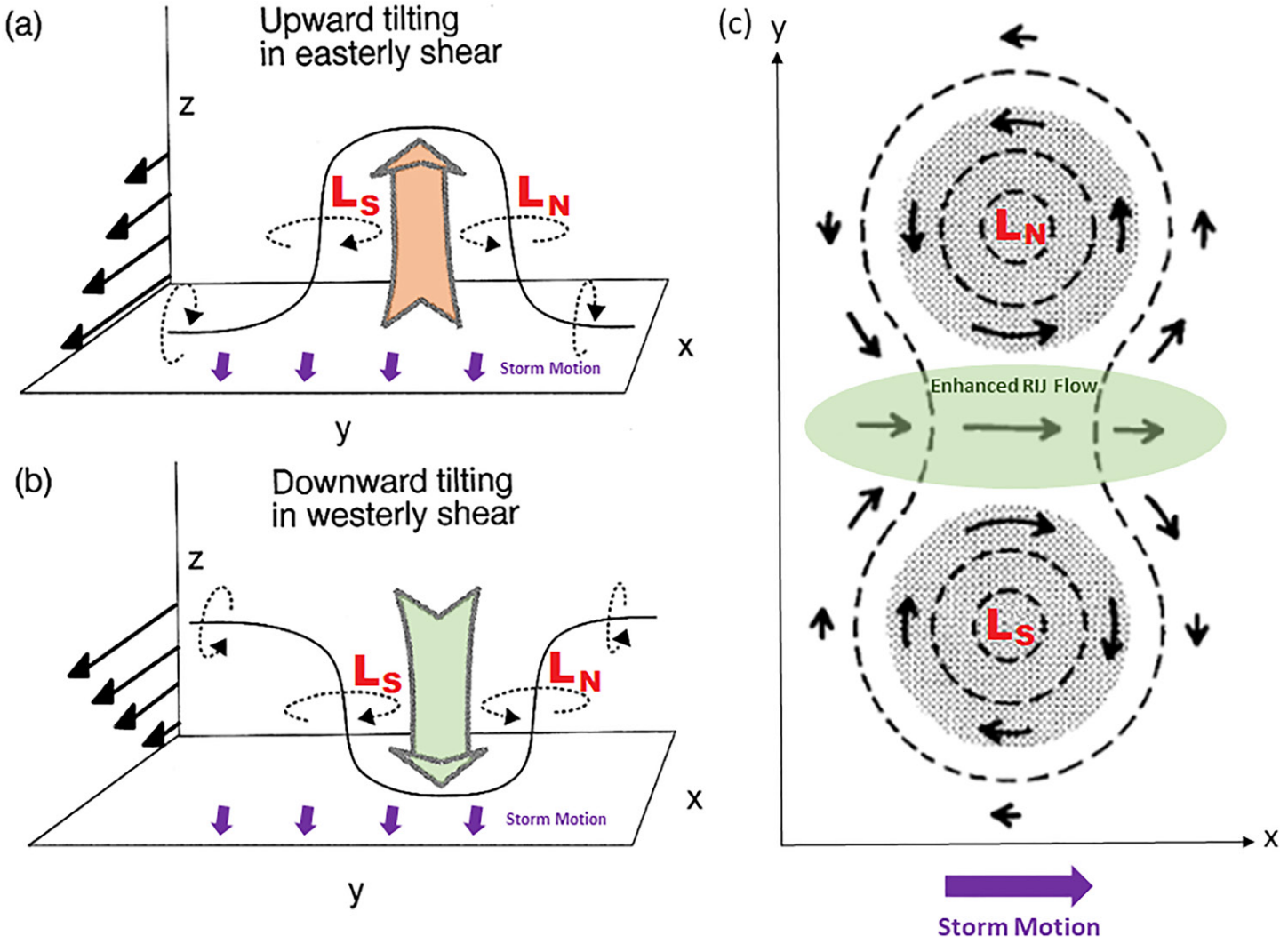

Fig. 8. Schematic of vertical vorticity generation through vortex tilting. In (a), ascending front-to-rear motion (as in Figs. 6, 8, and 9) or westerly shear pushes the vortex lines up in the center, resulting in cyclonic rotation on the north end (L_N) and anticyclonic rotation on the south end (L_S). In (b), descending motion from the RIJ (as in Fig. 8) or easterly shear produces the same vertical vorticity pattern. (c) A schematic representation of an idealized two-dimensional vortex couplet, depicting the stronger flow induced between the vortices. Gray shading denotes regions of constant vorticity. The green-shaded area shows where RIJ flow may strengthen due to an enhanced pressure gradient force induced between both book-end vortices. Unshaded regions have zero vorticity. Dashed contours represent an approximate negative pressure perturbation field that is consistent with the flow pattern. The letters denote the locations of the northern, dominant cyclonic (L_N) and southern, shorter-lived anticyclonic vortices (L_S). [The plots in (a) and (b) are adapted from Weisman and Davis (1998, Fig. 5) and (c) is adapted from Weisman (1993, Fig. 21).]

In this unique case, an intense nocturnal low-level jet supplied very strong low-level shear and associated streamwise vorticity to tilt and stretch into a powerful line-end mesovortex (Weisman et al. 2013; Evans et al. 2014).

RIJs may also support leading-line mesovortex development, which can support a DMCS's most damaging winds (Figs. 10a,b) (Trapp and Weisman 2003; Weisman and Trapp 2003; Atkins et al. 2004, 2005; Wheatley et al. 2006; Simon et al. 2011; Hamid 2012; Taszarek et al. 2019). Bow echo DMCSs can contain or evolve from supercells (Kleyla and Peterson 1990; Moller et al. 1994; Bernardet and Cotton 1998; Klimowski et al. 2004; Coniglio and Stensrud 2004) whose mesocyclones may evolve into leading-line mesovortices as a DMCS matures (Alfonso and Naranjo 1996; Dunn and Best 2011; Taszarek et al. 2019). The strongest leading-line mesovortices form on or north of the bow apex, with the destructive surface winds occurring on the south side of individual mesovortices, where both the RIJ and cyclonic vortical components of flow contribute to the total wind field (Figs. 10c–h) (Wakimoto et al. 2006b;

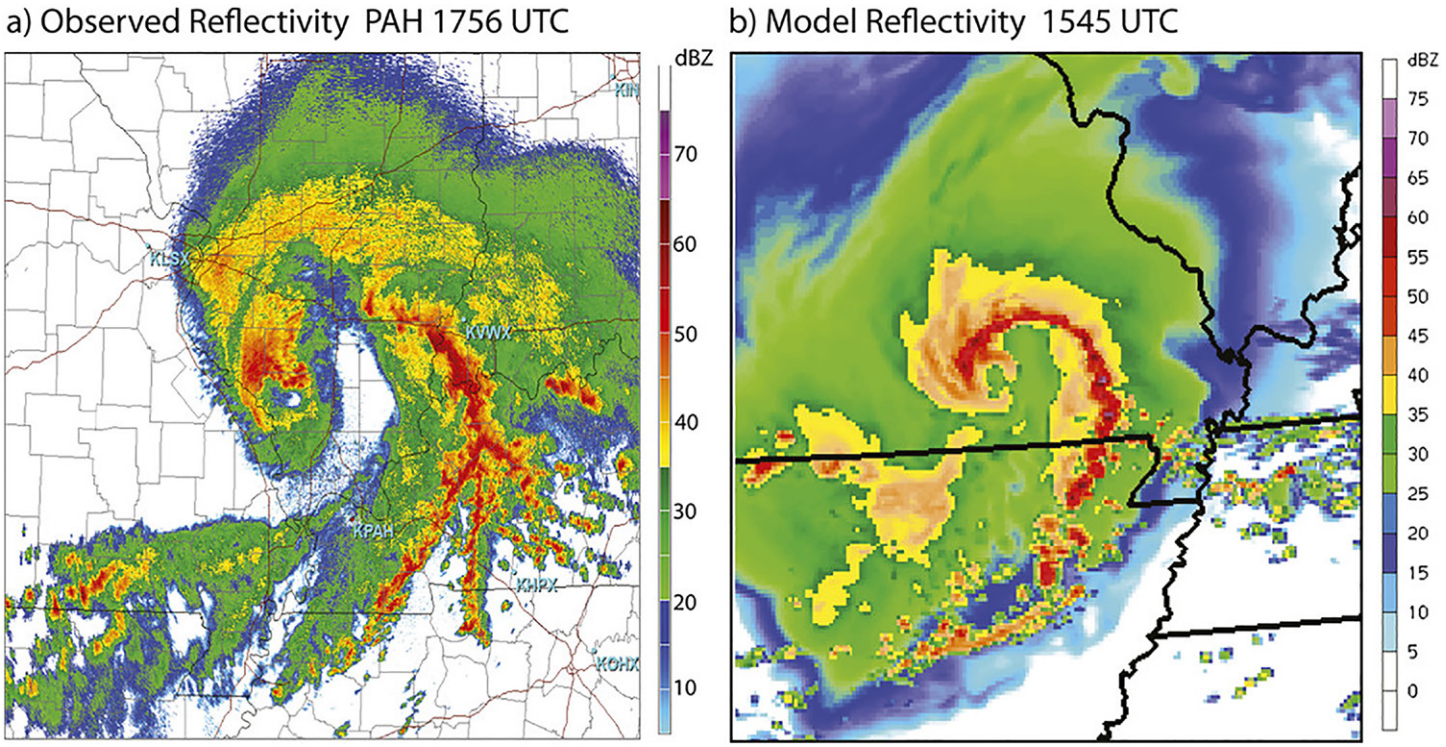

Fig. 9. (a) Paducah, Kentucky (PAH), Weather Surveillance Radar-1988 Doppler (WSR-88D) level II 0.5° radar reflectivity (dB*Z*) at 1756 UTC 8 May 2009. (b) Column maximum derived reflectivity (dB*Z*) from 27 h 3 km WRF-ARW real-time forecast, valid at 1545 UTC 8 May 2009. [From Weisman et al. (2013, Fig. 1).]

Atkins and St. Laurent 2009a; Atkins et al. 2005; Xu et al. 2015a). Leading-line mesovortices are generated when ambient and friction-induced vorticity is tilted by both upward front-to-rear flow and the downward RIJ, and then stretched by low-level convergence along the MCS leading line (Atkins and St. Laurent 2009b; Xu et al. 2015b; Flournoy and Coniglio 2019).

Atmospheric conditions favoring derecho development

Surface and upper-air patterns conducive to supporting progressive derechos. Johns (1984) attributed 90% of northwest-flow severe thunderstorm wind outbreaks to the presence of 50+ kt 500 hPa jet streaks, accompanied by under-10-dm height falls along an upper-level ridging pattern. Most of the studied severe events initiated north of a surface baroclinic zone, likely due to modest low-level warm-air advection triggered by the passage of a subtle 500 hPa shortwave trough embedded in the synoptic ridge. Johns and Hirt (1987, hereafter JH87) affirmed the synoptic setup in Johns (1984) to be the primary scenario for warm-season progressive DMCSs to occur across the climatologically favorable summertime corridor spanning from Minnesota to Ohio [see Figs. 8, 9, and 11a in Squitieri et al. (2023, hereafter Part I)]. Within this warm-season corridor, JH87 identified multiple meteorological parameters which favored warm-season progressive DMCS intensity and longevity for most of their 70 cases. The presence of northwesterly midlevel flow, strong low-level warm-air advection and wind speeds, a surface boundary, ample buoyancy, dry low to midlevels, and midlevel height falls all pointed to DMCS development. However, JH87 also pointed out that in the absence of either stronger midlevel-height falls, available buoyancy, or low-level dry air, DMCSs were only possible if all the other core criterion were met and stronger buoyancy was present over a longer corridor, with even lower RH at DMCS initiation.

Similar to JH87, Doswell and Evans (2003) found that northwesterly mid- to upper-level flow was prevalent in many weakly forced warm-season derecho cases, which contributed to elongated northwest-to-southeast-oriented hodographs (Fig. 11a). In many warm-season

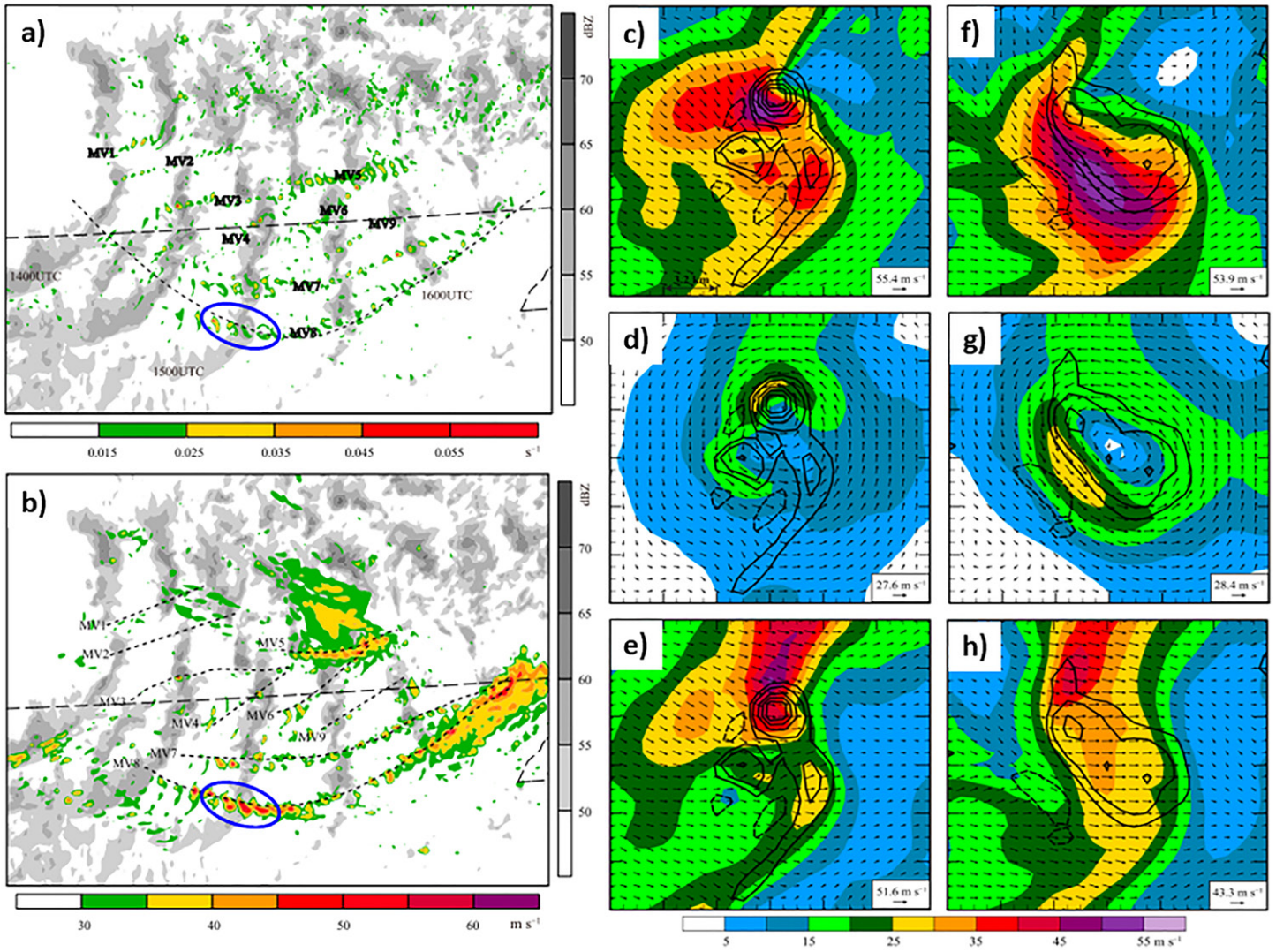

Fig. 10. WRF-ARW output of a real-case-based simulation of the 8 May 2009 central U.S. bow echo DMCS from 1400 to 1640 UTC, employing 0.8 km horizontal grid spacing. (a) Composite reflectivity (gray shading) and ground-relative tracks of the maximum absolute vertical vorticity below 2 km AGL (color shading). The thick dashed line denotes the approximate focus of the bow apex. Significant leading-line mesovortices are labeled. (b) As in (a), but that the color shading is for the ground-relative wind speed at 0.2 km AGL. Thin dashed lines are the tracks of leading-line mesovortices. Blue ellipses in (a) and (b) show the focused portions of the leading-line mesovortex (MV8) highlighted in the other panels. Decomposition of the (c) total ground-relative wind into (d) leading-line mesovortex-induced flow and (e) environmental flow at 200 m AGL at 1450 UTC. (f)–(h) As in (c)–(e), but for the wind at 1500 UTC. Vectors and shadings are for the ground-relative wind field and the corresponding wind speed. Black contour lines denote the simulated vertical vorticity at 200 m AGL at contour values of −0.005, 0.005, 0.01, 0.02, 0.03, and 0.04 s^{-1}, with dashed lines for negative values. The plotted domain is 19.2 km × 19.2 km. [The plots in (a), (b), and (c)–(h) are adapted from Figs. 12, 14, and 15, respectively of Xu et al. (2015a).]

cases, a 300–200 hPa jet streak often overspreads the strong 500 hPa flow (as shown in the 29 June 2012 case; Figs. 12a,b), with DMCSs frequently initiating at the upper-jet-streak right-entrance region, where ascent due to upper-level divergence is strongest. Beneath the stronger upper flow, a long west-to-east corridor of rich low-level moisture must be present for DMCS development and sustainment (Fig. 12c). The moisture deepens along a surface baroclinic boundary (Fig. 12d) and is overspread by an elevated mixed layer, characterized by dry air in the 850–500 hPa layer (Fig. 11b; weakly forced derecho relative humidity profile). The result is strong to extreme instability in an elongated corridor preceding the DMCS (as shown for the 10 August 2020 derecho; Fig. 13a), with lower downstream buoyancy supporting DMCS dissipation (Bentley et al. 2000; Coniglio and Stensrud 2001; Doswell and Evans 2003; Coniglio et al. 2004; Ashley et al. 2005, 2007). Steep midlevel lapse rates

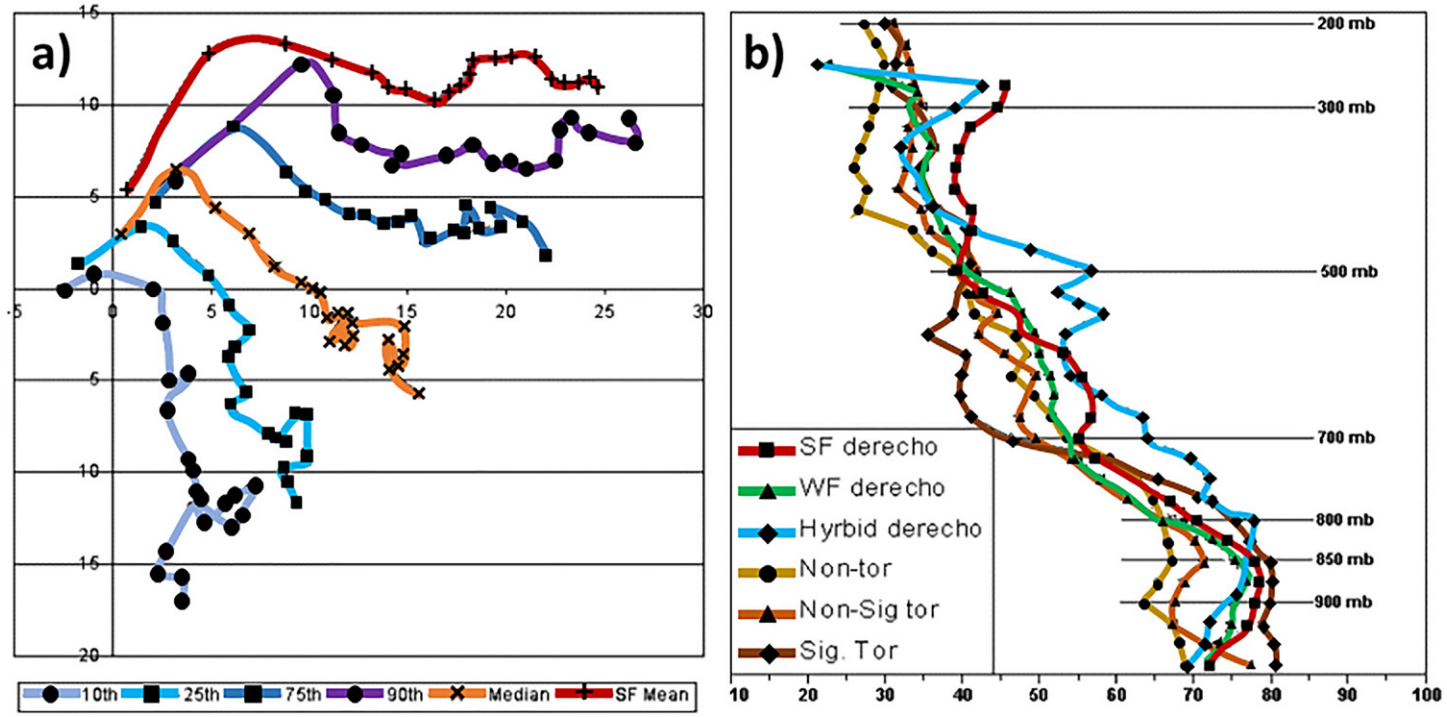

Fig. 11. (a) Comparison plot of the 10th-, 25th-, 50th (median)-, 75th-, and 90th-percentile hodographs for 51 weakly forced DMCSs, with the mean hodograph for 47 strongly forced DMCSs. (b) Mean vertical profiles of relative humidity (%) with pressure (hPa) for the three categories of supercells (nontornadic, weak tornadic, and significant tornadic) and the three categories of DMCSs (weakly forced, strongly forced, and hybrid). [The plots in (a) and (b) were adapted and subjectively augmented from Figs. 3 and 6, respectively, of Doswell and Evans (2003).]

(i.e., ≥8°C km^{-1}) comprising the elevated mixed layer contribute to wide CAPE profiles and resultant extreme instability (exemplified in an observed sounding ahead of the 10 August 2020 DMCS; Fig. 13b). Therefore, steep midlevel lapse rates are considered one of the most important ingredients for supporting DMCSs (Doswell and Evans 2003; Coniglio et al. 2012) and may have been key to supporting some of the most intense DMCSs in history (Coniglio et al. 2011; Bentley and Logsdon 2016).

While many studies agree that the ridging environment identified in JH87 supports DMCS maintenance, some studies noted substantial differences between synoptic features of warm-season progressive derecho events from the Plains states toward the Ohio Valley. Coniglio et al. (2004) identified three upper-level-ridging synoptic environments where DMCSs could form upstream, to the crest of, or downstream of the 500 hPa ridge (Fig. 14a). Maximum low-level moisture occurred at or downstream of DMCS initiation, with warm-air advection approaching from the south or southwest (Fig. 14b). DMCSs initiated either at the right-entrance region of a 250 hPa jet streak [similarly found by Clark et al. (2009) and Guastini and Bosart (2016)] or south of the jet max (Fig. 14c). Among the more weakly forced environments beyond JH87's classic ridging pattern (Figs. 15a–c), Guastini and Bosart (2016) noted that DMCSs formed in more broadly northwesterly flow regimes at the upper-jet right-entrance region across the eastern third of the contiguous United States (Figs. 15d–f), as also found for southeast-moving summertime DMCSs in Bentley et al. (2000). Even in more zonal upper-level flow environments (also identified in Coniglio et al. 2004), if low-level warm-air advection and upper-jet streak right-entrance divergence is strong enough, DMCSs may still develop, especially across the Ohio Valley (Figs. 15g–i). Across the Southern Plains, northwest flow regimes across the Rockies may support DMCS development amid surface lee-troughing or cyclone development (Figs. 15j–l). Many of these ambient environments, though similar, stray enough from the classic JH87 synoptic framework such that

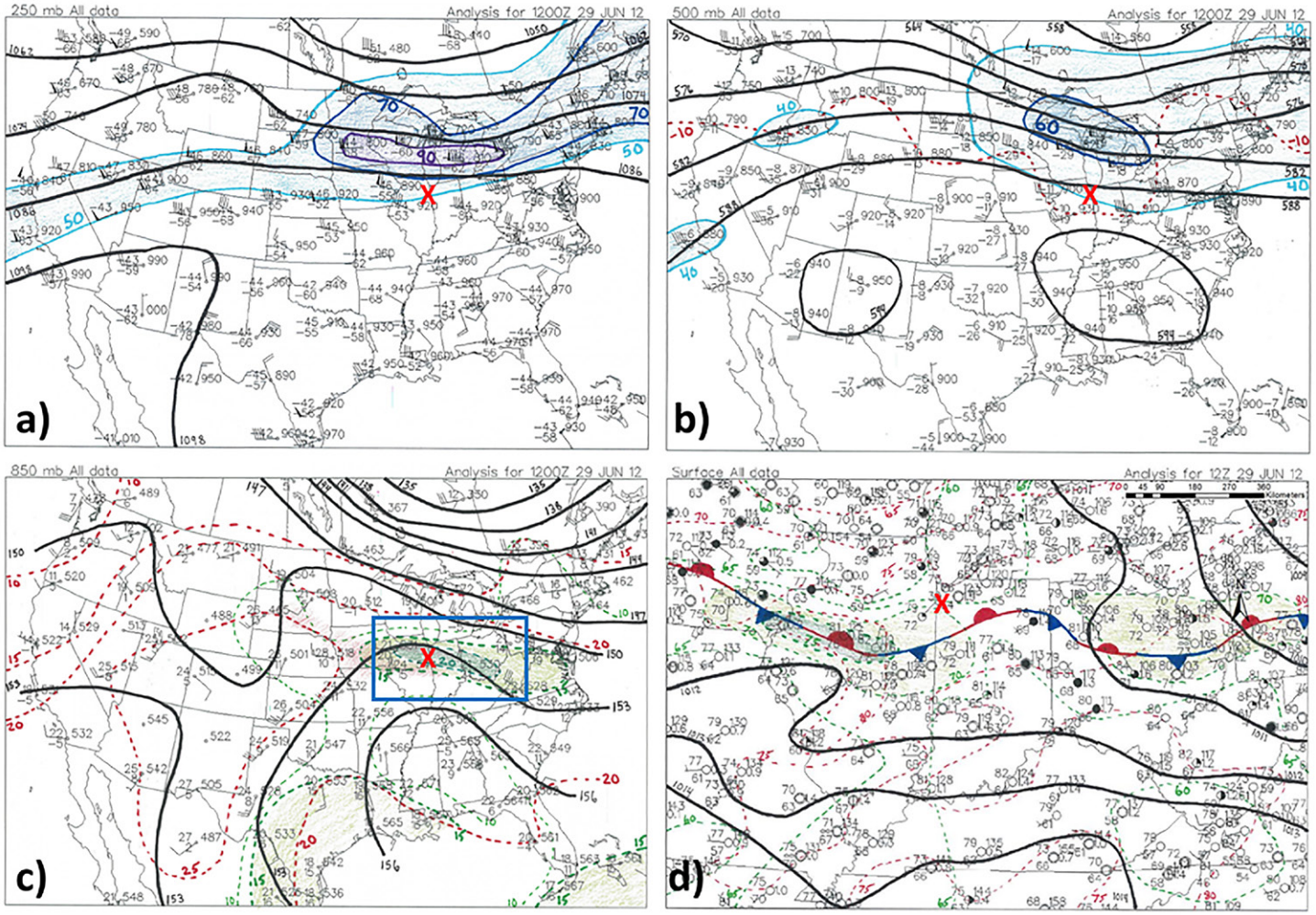

Fig. 12. Hand analyses maps of observed data for 1200 UTC 29 Jun 2012, showing (a) 250 hPa observations with black isohypses every 120 m, and light blue, dark blue, and purple isotachs showing 25 m s^{-1} (50 kt), 36 m s^{-1} (70 kt), and 46 m s^{-1} (90 kt) wind speeds, respectively. (b) 500 hPa observations with black isohypses every 60 m, red dashed isotherms every 10°C, and with light and dark blue isotachs representing 20 m s^{-1} (40 kt) and 30 m s^{-1} (60 kt) wind speeds, respectively. (c) 850 hPa observations with black isohypses every 30 m, red dashed isotherms every 5°C, and shaded isodrosotherms > 10°C (light and dark green shades represent >15° and 20°C, respectively). Light-red shading from South Dakota into Illinois represents warm-air advection. The blue box focuses on the surface analyses. (d) Surface observations with black mean sea level isobars every 1 hPa, red isotherms every 5°F (2.8°C), and shaded isodrosotherms over 70°F (21°C) every 5°F (2.8°C). A hand-drawn surface baroclinic zone extends from Iowa to Pennsylvania. The red "X" symbols in all plots estimates placement of DMCS initiation. [The plots in (a), (b), (c), and (d) were adapted from Figs. 2, 3, 5, and 6, respectively, of Bentley and Logsdon (2016).]

Guastini and Bosart (2016) discouraged relying solely on the JH87 conceptual model of warm-season progressive derechos.

Observational-based studies have suggested strong buoyancy, in combination with strong deeper-layer shear (i.e., from the surface up to 6 km AGL), are useful discriminators between weaker MCSs versus bow echoes and DMCS events (Cohen et al. 2007; Mauri and Gallus 2021; Gallus and Duhachek 2022). Multiple studies found that strong shear should counter the cold pool through a deeper layer (up to 5 km AGL in some cases) for the more intense MCSs (Garner and Thorpe 1992; Szeto and Cho 1994; Fovell and Dailey 1995; Weisman and Rotunno 2004; Coniglio et al. 2006, 2012) since some cold pools could become over 4 km deep (Bryan and Rotunno 2008; Bryan and Parker 2010). It is likely that stronger line-normal shear in roughly the 3–4 km AGL layer above the cold pool may be needed to compensate for the weaker line-normal low-level component of shear to maintain convection along the cold-pool leading edge in some cases (Parker and Johnson 2004; Coniglio et al. 2006). Still, some observational studies (i.e., Cohen et al. 2007), which showed deep-layer shear as a good

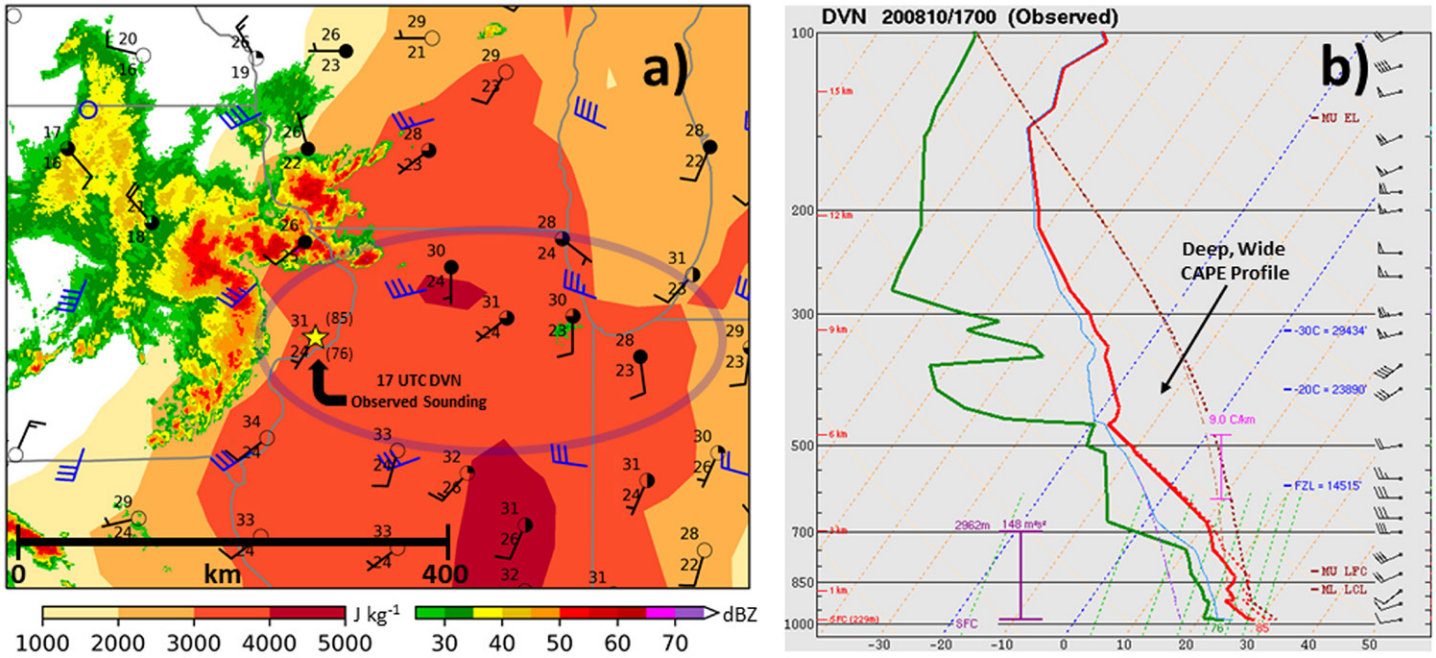

Fig. 13. (a) Planar map (valid 1700 UTC 10 Aug 2020) showing composite reflectivity overlaid with surface observations (top and bottom numbers at each station correspond to temperatures and dewpoints in °C; wind barbs in kt; and filled dots indicating the level of cloud cover), MLCAPE (J kg^{-1}; shaded) and effective bulk shear (kt; blue wind barbs). MLCAPE and effective bulk shear values were derived from the 1700 UTC Surface Objective Analysis. The yellow star indicates the location of the 1700 UTC Davenport, Iowa (DVN), observed sounding, with the top and bottom numbers in parentheses at the DVN ASOS cite corresponding to the 1700 UTC observed-sounding surface temperatures and dewpoints (in °F), respectively. A distance scale was provided for reference. The translucent ellipse across northern Illinois into northwest Indiana highlights the elongated corridor of overlapping strong buoyancy and effective bulk shear. (b) 1700 UTC 10 Aug 2020 DVN nonroutine observed sounding taken ahead of the parent DMCS.

discriminator between intense wind-producing MCSs and low-end cases, also found that storm relative low-level inflow was an excellent discriminator between higher-end wind producing MCSs and weaker events. Alfaro (2017) expanded on the findings of Cohen et al. (2007), noting that stronger low-level shear supported a relatively greater influx of buoyant air in the layer of inflow (Figs. 1 and 3c), which favored stronger MCSs. Mulholland et al. (2021) further showed that stronger low-level shear not only increased an MCSs inflow of convectively unstable air, but also reduced the amount of dilution and weakening of thunderstorm updrafts from midlevel dry-air entrainment. While Mauri and Gallus (2021) did not find a strong correlation between low-level shear and nocturnal bow echo MCS intensity, they did find that the best discriminator between nighttime derecho-supporting bow echoes and weaker events were composite parameters which consisted of variables involving low-level shear, deep-layer shear, and buoyancy. The findings of Alfaro (2017) and Mulholland et al. (2021) showing low-level shear directly influencing buoyant inflow and midlevel dry-air entrainment may explain why composite parameters in Mauri and Gallus (2021) were the best predictors for stronger nocturnal bow echoes (including DMCSs).

While multiple studies have found that varying synoptic environments can support warm-season derechos, and while arguments exist among some studies regarding whether low-level versus deeper-layer shear is more important to warm-season DMCS organization and sustenance, one commonality among most studies is that a DMCS must be preceded by a long corridor of overlapping strong to extreme instability and adequate vertical shear that is aligned with DMCS forward motion (JH87; Bentley et al. 2000; Coniglio et al. 2004; Bentley and Logsdon 2016). Based on decades of research, it is clear that a long corridor of favorable buoyancy and shear is the first signal forecasters should look for, which enables a DMCS to organize and produce the long wind-damage swath which characterizes derechos.

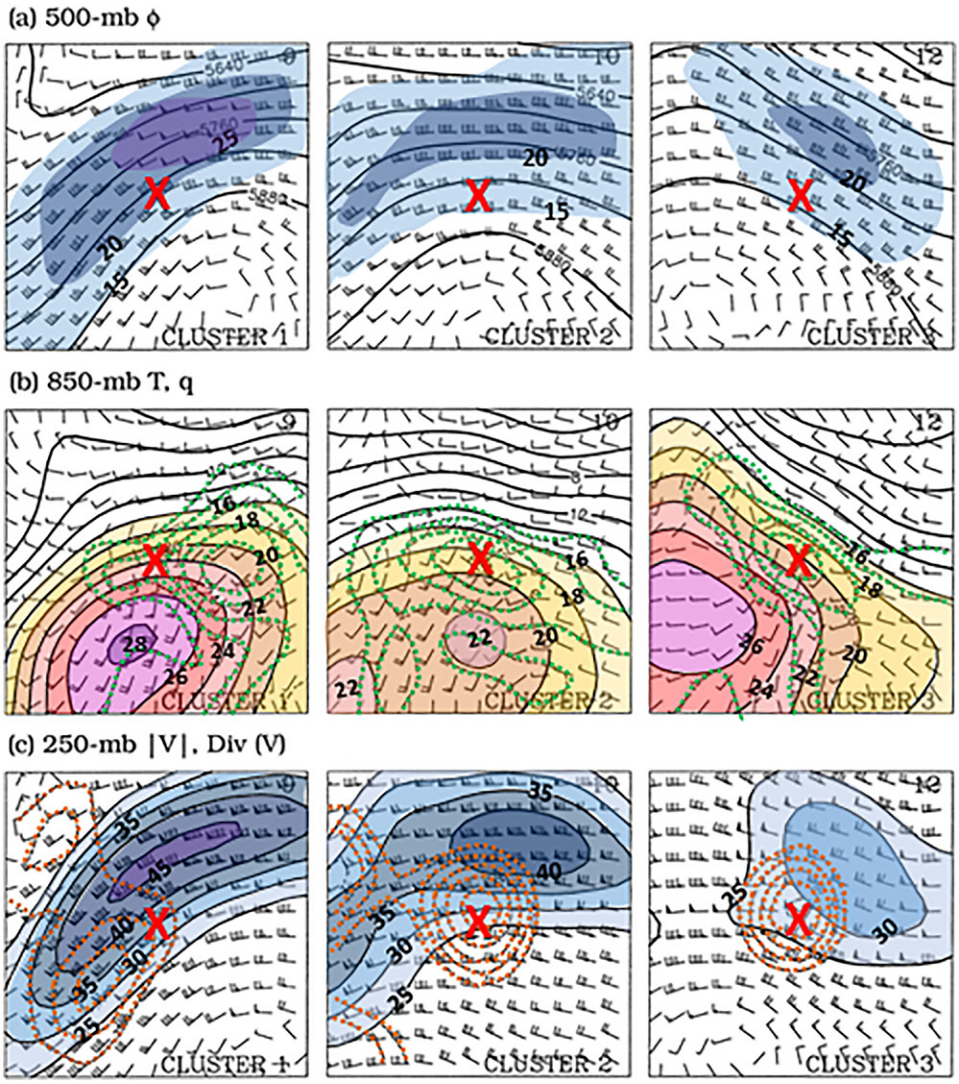

Fig. 14. A composite plot of multiple warm-season DMCS environments driven by upper ridging, showing (a) the mean 500 hPa geopotential height (ϕ; contours every 60 m), wind (flag: 50 kt or 25 m s^{-1}; full barb: 10 kt or 5 m s^{-1}), and wind speed ($|V|$; shaded every 5 m s^{-1}, starting at 15 m s^{-1}) for three clusters within the upper-ridging pattern. (b) As in (a), but for the 850 hPa temperature (T; solid contours every 2°C, with shading for values over 16°C) and specific humidity (q; green dashed contours every 1 g kg^{-1} starting at 8 g kg^{-1}). (c) As in (a), but for the 250 hPa wind speed [$|V|$; shaded every 5 m s^{-1}, starting at 25 m s^{-1}; divergence of the wind Div(V); orange dashed contours every 0.25 × 10^{-5} s^{-1}]. The horizontal and vertical dimensions of each grid are 2600 km and 2400 km, respectively. The "X" symbol denotes the mean position of the DMCS at the analysis time. The number of cases comprising a cluster for each synoptic pattern (left) 9, (center) 10, and (right) 12. [Subjectively augmented from Coniglio et al. (2004, Fig. 7).]

Warm-season progressive DMCSs occurring in series. Multiple studies in the last 40 years have noted that summer DMCSs can occur in series, both in the United States (Johns 1982; Bentley and Sparks 2003; Ashley et al. 2005, 2007; Metz and Bosart 2010; Lyza et al. 2017) and in Europe (Surowiecki and Taszarek 2020). Johns (1982) noted that for northwest flow summer severe outbreaks (most of which were severe wind events), there was a 50% chance that an outbreak would be followed by a second event and a 20% chance that more than two events would follow. Defining a DMCS series as more than one event occurring within 72 h in similar synoptic environments, Ashley et al. (2005) noted that DMCS series comprised three events on average, with multiple series containing four to six DMCSs, and two series events (June 1998 and July 2003) having nine DMCSs in a row (Fig. 16a). Ashley et al. (2005) also found that most of the 1994–2003 DMCS series occurred in May–July (Fig. 16b). Eighty-two percent of all May–July DMCSs occurred in series

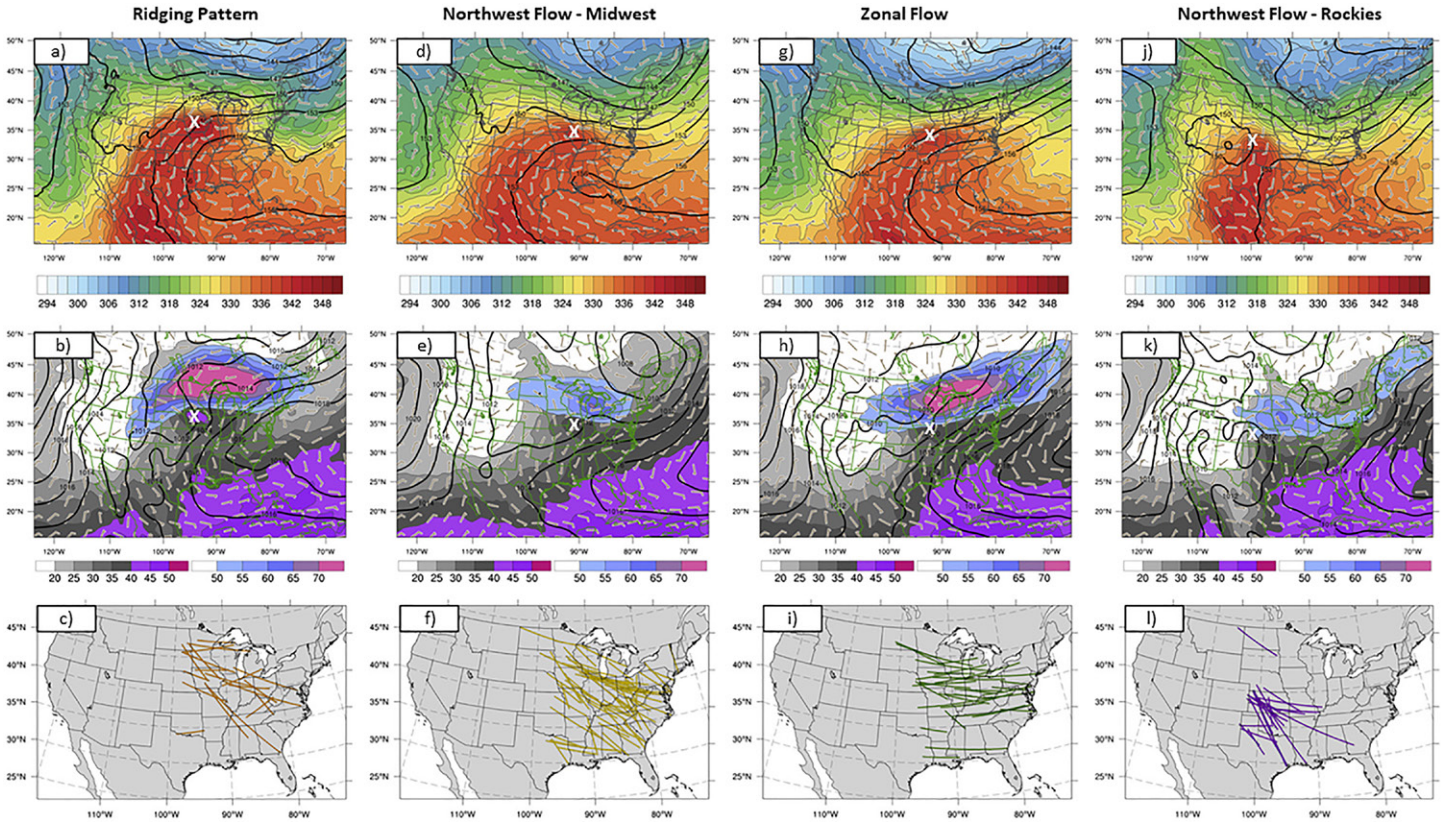

Fig. 15. Composite synoptic fields from the Climate Forecast System Reanalysis of four synoptic environments favoring DMCS development, including (a)–(c) upper ridging, (d)–(f) northwest flow driving Midwest events, (g)–(i) zonal flow, and (j)–(l) northwest flow driving events in the Plains. (top) Composite 850 hPa geopotential height (contours; dam), 850 hPa winds (barbs; kt), and 850 hPa θ_e (color fill; K). (middle) Composite mean sea level pressure (contours; hPa), precipitable water (gray fill; mm), 250 hPa wind magnitude (color fill; kt), and 1000 hPa winds (barbs; kt). (bottom) Lines connecting the starting and ending points of each derecho in their respective environments. The white "X" symbols in the top and middle rows are located at the composite DMCS initiation location to which each member grid was shifted before averaging over all category members. [The plots in (a)–(c), (d)–(f), (g)–(i), and (j)–(l) are adapted from Figs. 11, 12, 13, and 16, respectively, of Guastini and Bosart (2016).]

annually, and that 75% of all series events occurred within the May–July period. In these three months, a 58% chance existed for a DMCS to be followed by a second event, and a 46% chance that a third DMCS would occur. Though Ashley et al. (2005) identified relative derecho maxima spanning from the Ohio Valley to the Southern Plains (Fig. 16c), the number of individual DMCSs within a series (Fig. 16d), the number of total DMCS series (Fig. 16e), and number of DMCS series with three or more events (Fig. 16f) were highest along the northern summer derecho corridor extending from the Upper Mississippi Valley to the Ohio Valley.

A persistent upper-level ridge and corresponding convective inhibition above the planetary boundary layer can support prolonged favorable conditions for DMCSs during the summer. As rich low-level moisture builds beneath the cap, appreciably large buoyancy becomes available over extended time frames, supporting the potential for a DMCS series, as in 1998, where a record number of derechos occurred in May–June (Ashley et al. 2007). A DMCS series can unfold under three scenarios. In a "direct" DMCS series, initial DMCSs can generate outflow boundaries or gravity waves, which in turn serve as sources of lift for initiation or intensification of subsequent DMCSs. "Indirect" DMCS series occur when individual DMCSs within the series are initiated independently from preceding events. For example, individual DMCSs may initiate with multiple passing midlevel perturbations embedded within a large-scale upper ridge along a wide east–west corridor of strong instability and deep-layer shear. Finally, a DMCS series may encompass multiple DMCSs initiated by both direct and indirect means (Ashley et al. 2007).

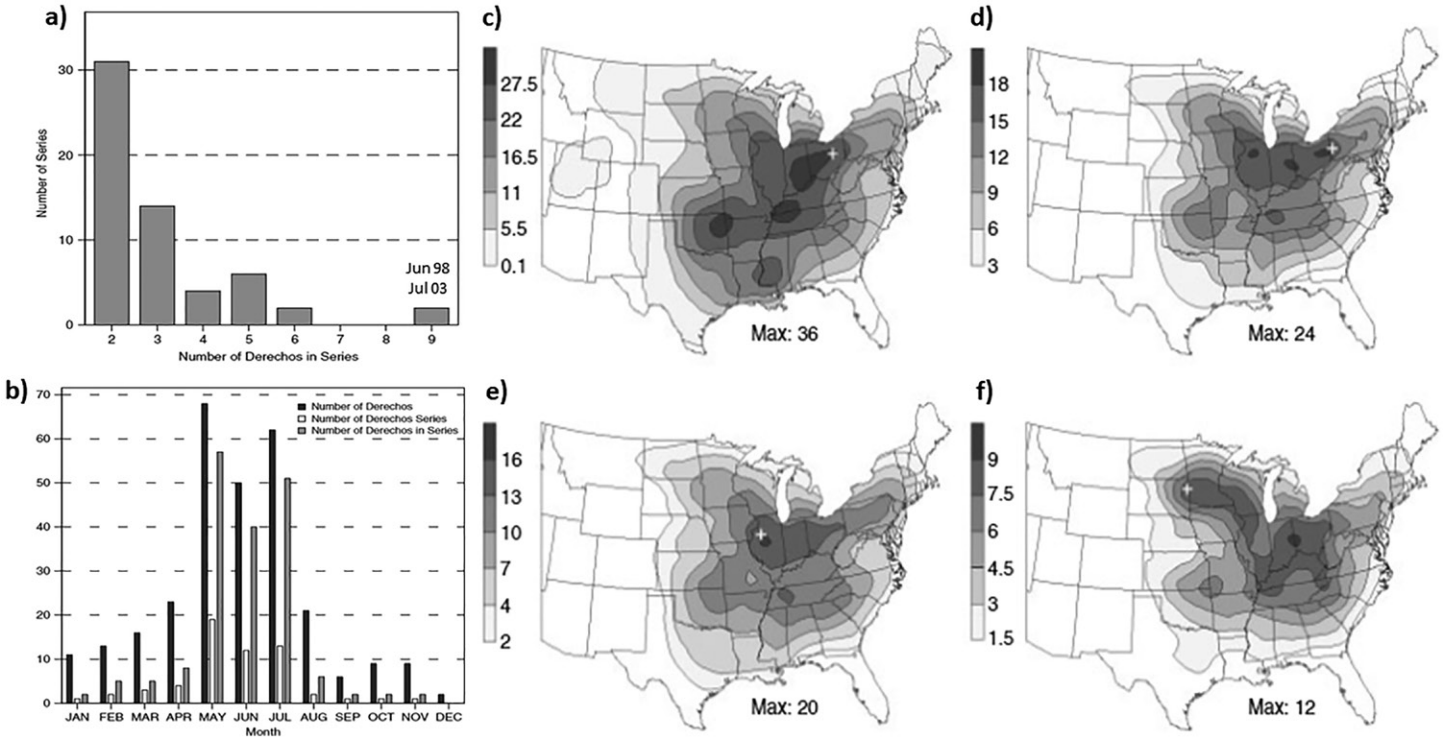

Fig. 16. (a) The frequency of series by the number of DMCSs in a grouping. (b) The number of DMCSs, DMCS series, and events in a series by month. Areal distribution of (c) DMCSs, (d) DMCSs within a series, (e) number of DMCS series, and (f) DMCS series with 3+ events across the contiguous United States. Symbols indicate the location of maximum values before interpolation. Derecho statistics are for the 1994–2003 period. [The plots in (a), (b), and (c)–(f) are from Figs. 4, 5, and 7, respectively, of Ashley et al. (2005).]

Strongly forced and "hybrid" derecho synoptic environments. Unlike progressive DMCSs, JH87 noted that serial DMCSs are strongly forced, are often initiated off of strong cold fronts, and are sustained by the low-level convergence of a surface cyclone and deep-layer ascent by coupling lower and upper jet streams (Coniglio et al. 2004), much like the severe weather patterns identified in Uccellini and Johnson (1979). As such, most serial-derecho environments resemble those of tornado outbreaks (Bentley and Mote 2000; Burke and Schultz 2004), and usually occur during the cool season across the Southeast into the Ohio Valley (see Figs. 11b,d in Part I). While Coniglio et al. (2004) found slight differences among strongly forced derecho regimes, all serial DMCSs formed ahead of a 500 hPa shortwave trough and to the south of a 250 hPa divergence maximum, with low-level warm air and moisture advection immediately preceding serial DMCS initiation (Fig. 17), as also found by Burke and Schultz (2004) for cool-season bow echo MCSs.

Though not always mutually exclusive, the primary synoptic differences between serial derecho and some tornado outbreak environments is that serial DMCSs benefit from more unidirectional vertical wind profiles (Coniglio et al. 2004) and a drier boundary layer (Ashley et al. 2007), often driven by veering 850 hPa winds (Johns 1993). These conditions support linear storm structures, stronger evaporative cooling, and more effective downward momentum transport, contributing to relatively greater and more widespread severe wind potential (Bentley and Mote 2000). With strong squall-line-parallel deep-layer flow, strongly forced DMCSs tend to occur with longer hodographs compared to weakly forced DMCSs (Fig. 18a) and straighter hodographs compared to significant tornado environments (Fig. 18b) (Bentley and Mote 2000; Doswell and Evans 2003; Coniglio et al. 2004). Since stronger forcing and shear often accompany serial and hybrid derecho environments, the parameter space (especially buoyancy) needed to support such events varies more widely compared to progressive derechos (Evans and Doswell 2001; Doswell and Evans 2003; Coniglio et al. 2004).

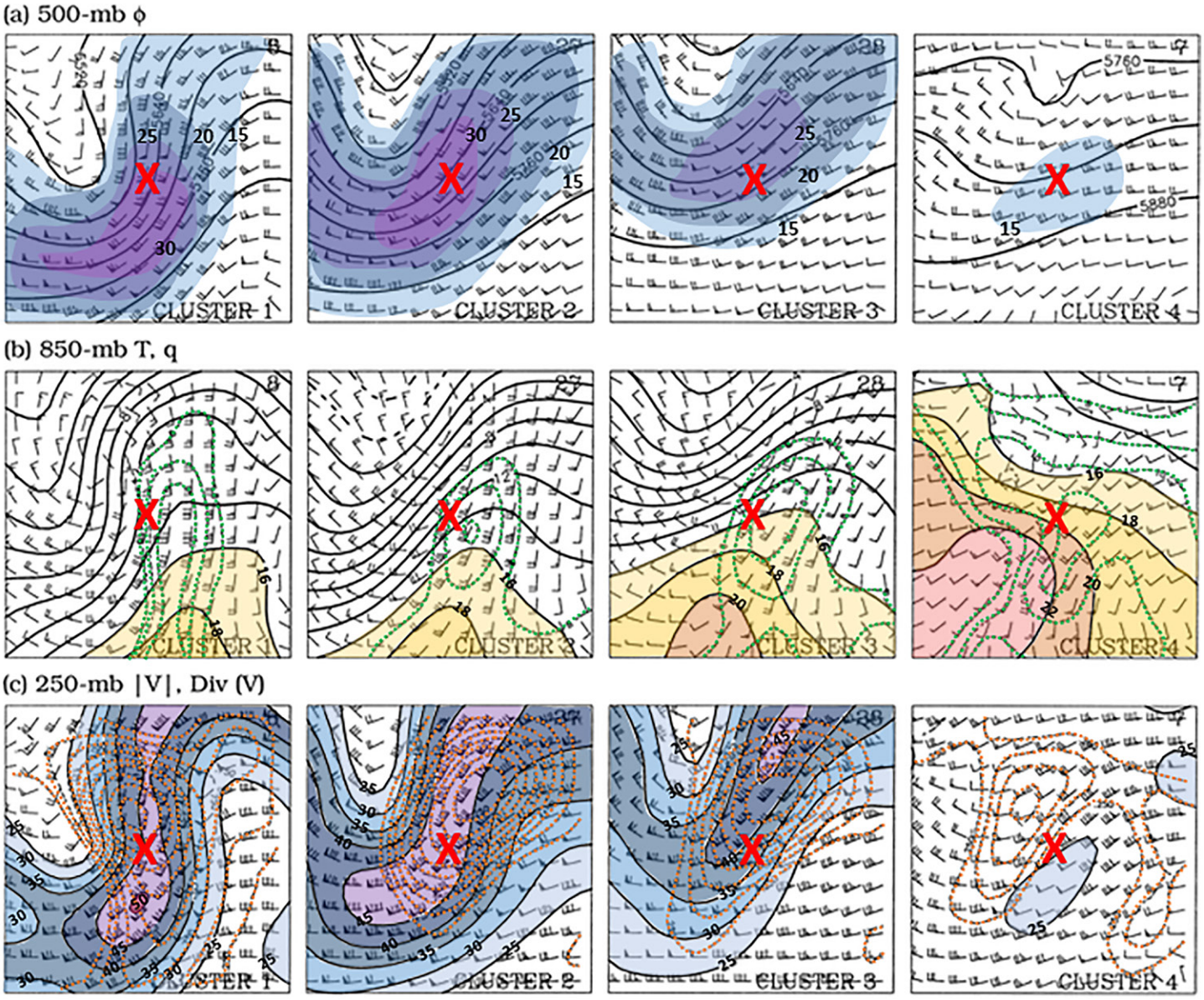

Fig. 17. As in Fig. 14, but for strongly forced DMCSs initiated in upper-troughing environments. The number of cases comprising a cluster for each synoptic pattern are (left to right) 8, 27, 28, and 7, respectively. [Subjectively augmented from Coniglio et al. (2004, Fig. 6).]

Stronger-forced DMCSs are usually accompanied by less CAPE (Fig. 18c) compared to weakly forced events (Bentley and Mote 2000), oftentimes thriving with CAPE values around or less than 1,000 J kg^{-1} in both the United States and Europe (Burke and Schultz 2004; Gatzen et al. 2020), especially when low to midlevels are dry (Punkka et al. 2006; Sipos et al. 2021).

While cool-season serial derecho and warm-season progressive derecho environments are distinguishable, multiple studies have described "hybrid" derecho environments. In hybrid cases, either serial (squall line) DMCSs developed in synoptic environments similar to warm-season events (as in Duke and Rogash 1992) or progressive (bow echo) DMCSs developed amid upper troughing, often with a northeasterly storm motion, as seen in many European derecho studies (Gatzen 2004; López 2007; Hamid 2012; Celiński-Mysław and Matuszko 2014; Taszarek et al. 2019; Gatzen et al. 2020; Surowiecki and Taszarek 2020; Chernokulsky et al. 2022). In the United States, Coniglio et al. (2004) noted that 28% of their cases were hybrid events, which encompasses synoptic environments that showed a combination of upper-ridging and -troughing characteristics (a blend of Figs. 10 and 13). Guastini and Bosart (2016) similarly noted warm-season progressive DMCSs accompanied

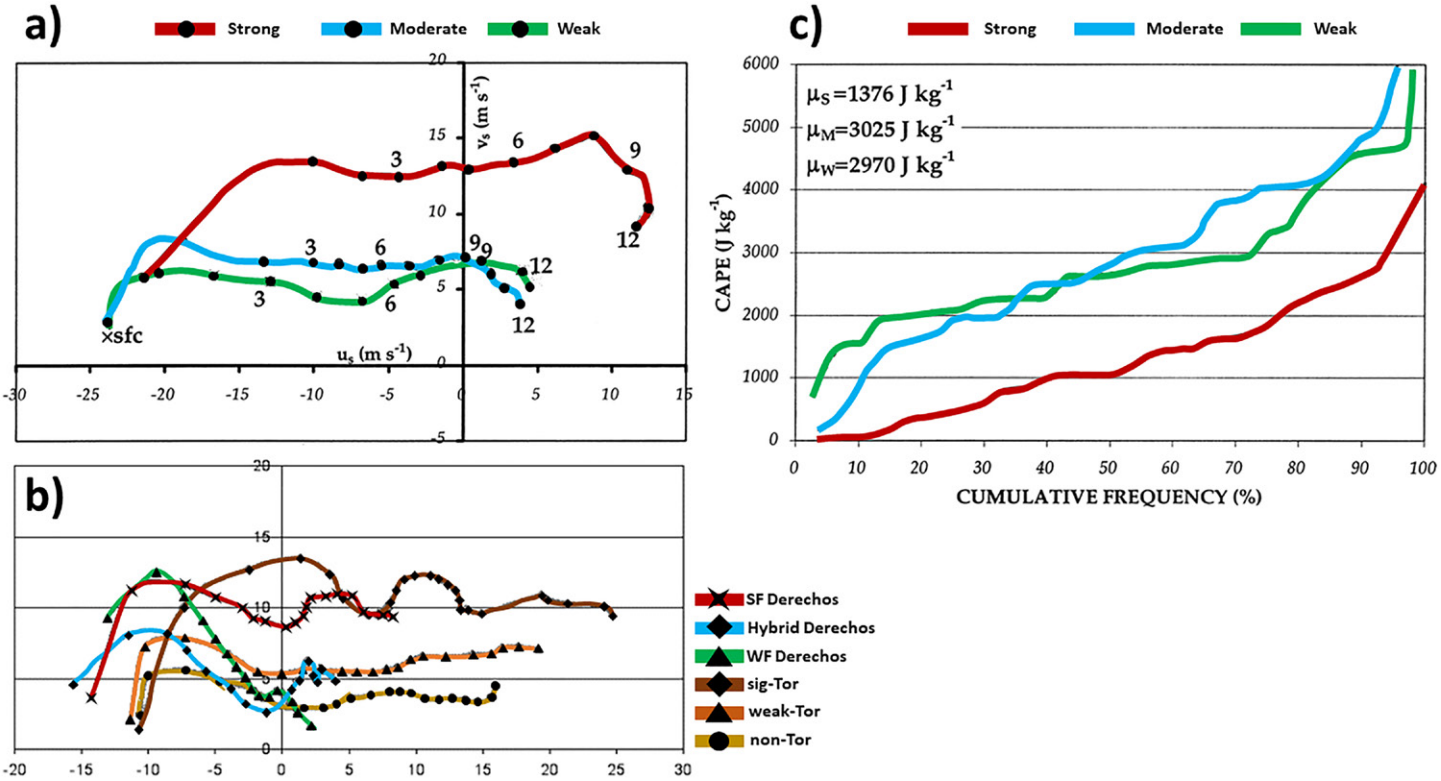

Fig. 18. (a) Mean hodographs for strongly, moderately, and weakly forced DMCS soundings. Prior to averaging, the wind components (u, v) in each sounding are represented in a coordinate system with the tip of the mean MCS motion vector (u_s, v_s) at the origin. The mean storm-relative winds are calculated every 0.5 km AGL, are plotted every 1 km AGL, and are labeled every 3 km AGL. (b) Comparison of mean hodographs using storm-relative winds for the nontornadic, weak tornadic (<F2 rating), and significant (≥F2 rating) tornadic supercell categories, and the weakly forced, strongly forced, and hybrid DMCS categories. Hodograph plot shows the u component along the ordinate and the v component along the abscissa (both in m s^{-1}). (c) The cumulative frequency distribution of CAPE (J kg^{-1}) for strongly, moderately, and weakly forcing soundings. The sample means for the strongly (μ_S), moderately (μ_M), and weakly forcing (μ_W) soundings are shown in the upper-left corner. [The plots in (a)–(c) are adapted and subjectively augmented from Coniglio et al. (2004, Fig. 17), Doswell and Evans (2003, Fig. 9), and Coniglio et al. (2004, Fig. 15), respectively.]

by upper troughs and surface lows, particularly over the U.S. Great Plains, with a subset of DMCSs bearing a northeasterly direction (Fig. 19), similar to Bentley et al. (2000). However, unlike Coniglio et al. (2004), Guastini and Bosart (2016) did not label these environments as hybrid, demonstrating that there is some ambiguity in how the "hybrid derecho" terminology is applied.

Derechos in dry deep-layer environments. On rare occasions, DMCSs can develop in deep, dry boundary layer environments. Few such cases have been documented in the literature, with a few events recognized in the United States (Corfidi et al. 2006, 2016), eastern Europe (Sipos et al. 2021), and arid portions of northwest China (Takemi 1999). "Low-dewpoint derechos" identified by Corfidi et al. (2006, 2016) occur in strongly forced environments, with convective initiation associated with a cold front and accompanying upper trough. The ambient thermodynamic environment preceding these DMCSs is characterized by narrow, short CAPE profiles atop a dry boundary layer several hundred hPa deep (Fig. 20), resembling the dry microburst soundings referred to by Wakimoto (1985). For the western U.S. cases, Corfidi et al. (2016) noted that the derecho wind swaths were associated with convective line segments ahead of the most progressive portion of the advancing surface cold front and corresponding convective cold pool. The presence of strong speed shear atop the MCS cold pool increased cell mergers and upscale growth along the MCS leading line. The cold pool would then spread in the direction of the deep-layer speed shear vector, with

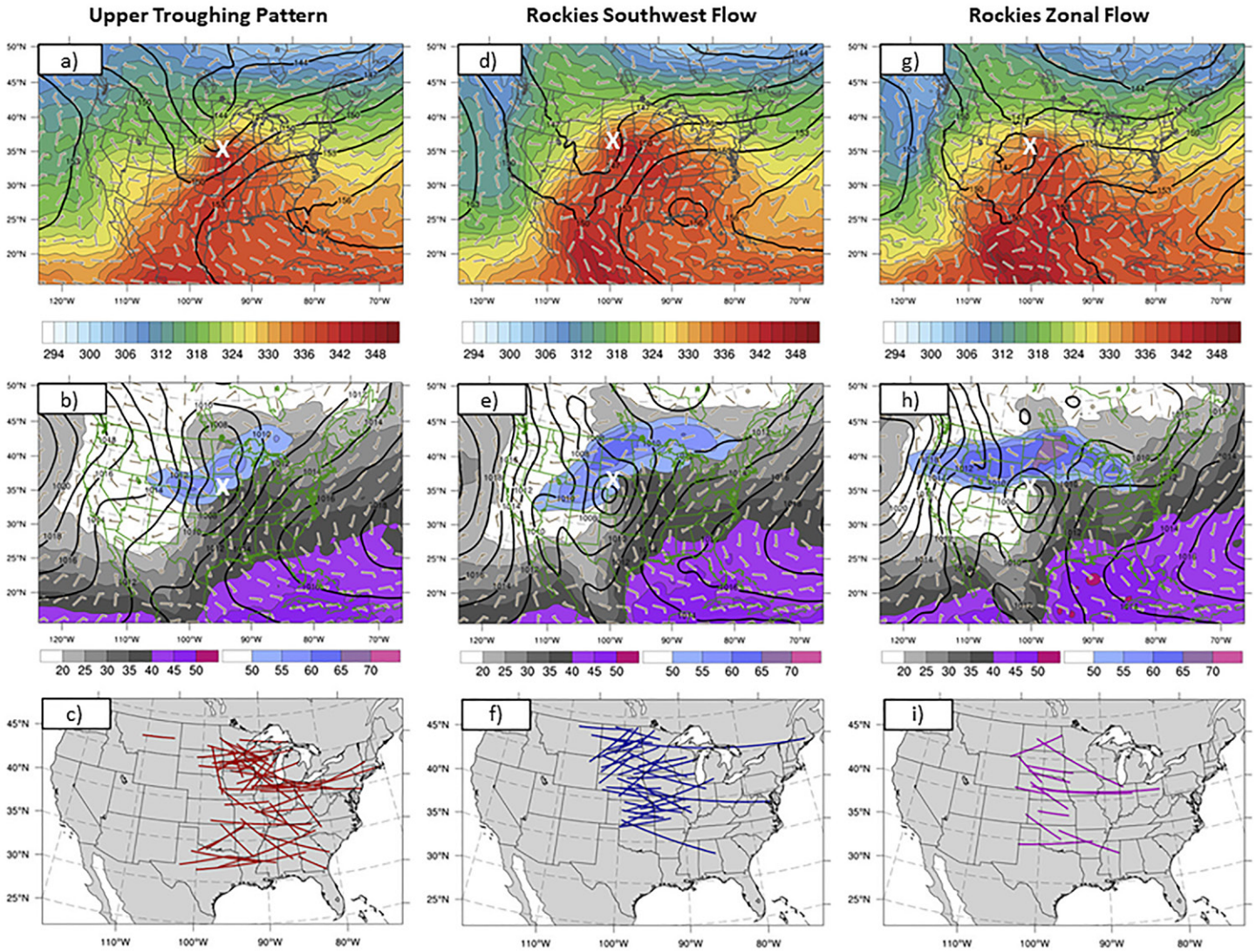

Fig. 19. As in Fig. 15, but for (a)–(c) upper-level troughing pattern, (d)–(f) southwest flow across the Rockies, and (g)–(i) zonal flow across the Rockies. [The plots in (a)–(c), (d)–(f), and (g)–(i) are adapted from Figs. 14, 15, and 17, respectively, of Guastini and Bosart (2016).]

derecho-longevity achieved as DMCS propagation becomes aligned with the mean wind. On the other hand, the 17 September 2017 DMCS across Romania and Serbia featured in Sipos et al. (2021) occurred in a weakly forced/sheared environment, but with steep boundary layer lapse rates. The derecho-like event across arid northwest China on 5 May 1993 also occurred with weak low-level shear, a very deep, well-mixed boundary layer, and rapidly progressed with the aid of a strong cold pool (Takemi 1999). Steep boundary layer lapse rates were the common atmospheric feature associated with nearly all the low-dewpoint derechos studied by Corfidi et al. (2006, 2016) and Sipos et al. (2021), suggesting that the downward acceleration of evaporatively cooled air parcels in a well-mixed boundary layer are key storm-scale factors driving low-dewpoint derechos.

Challenges and successes in simulating DMCSs in numerical weather models

Improvements have been made in derecho forecasts with the advancement in numerical model guidance over the last 20 years, especially with the employment of convection-allowing models (CAMs). Before CAMs were used widely, Gallus et al. (2005) attempted to simulate the 4 July 1999 DMCS with an ensemble framework of 25 members from three model cores, with a variety of convective parameterization schemes, initial conditions, and 4–10 km horizontal

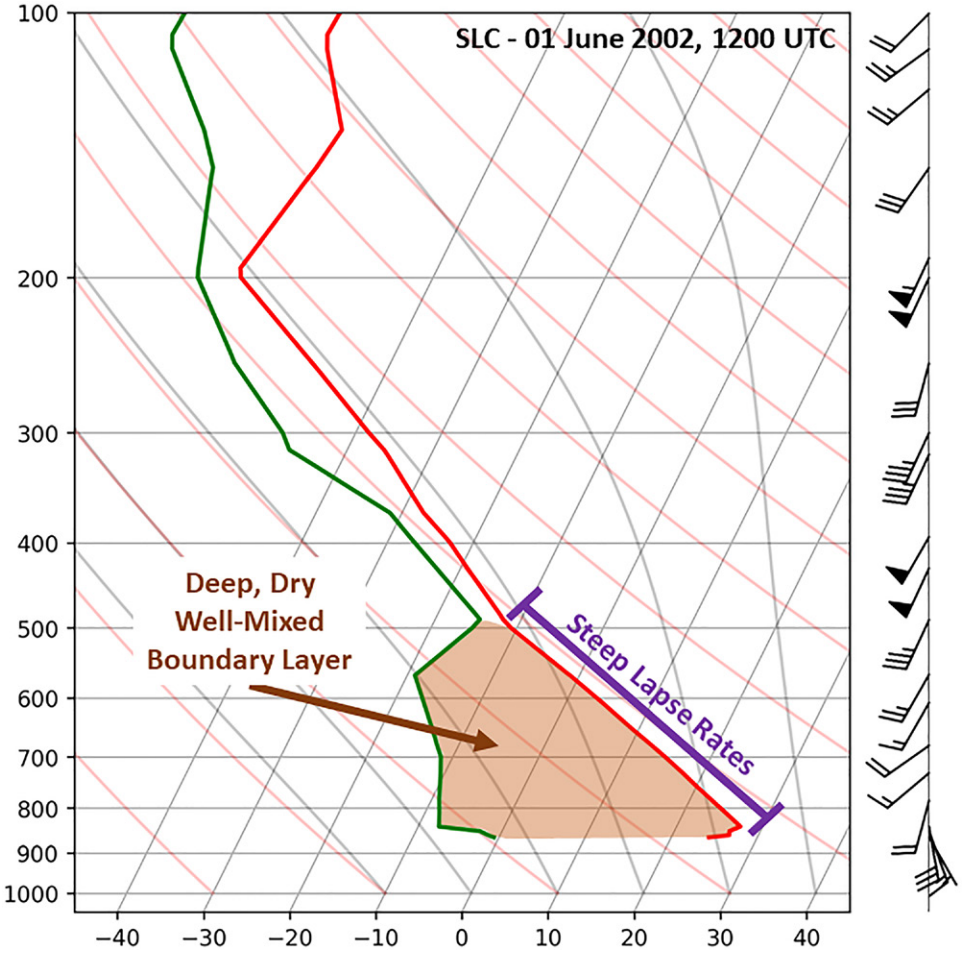

Fig. 20. Skew *T*–log*p* radiosonde temperature and dewpoint profiles for Salt Lake City, Utah (SLC), at 1200 UTC (red and green lines, respectively) 1 Jun 2002. Vertical wind profile (kt; 1 kt ≈ 0.51 m s^{-1}) shown to the right of the skew *T*, using conventional barb format, with surface air and dewpoint temperatures (°C) at bottom. [Same skew *T* featured in Corfidi et al. (2016, Fig. 15).]

grid spacings (Δx) employed. No ensemble member could simulate the DMCS, likely due to a lack of observations to initialize models, poor data assimilation, and ability to resolve the storm-scale mechanisms (i.e., strong cold pools, RIJs, mesovortices, etc.) needed to organize a DMCS and support a derecho wind swath. Similarly, non-CAM simulations by Púčik et al. (2011) failed to depict the development of a mesolow (as seen from observations) and subsequent DMCS development across central Europe for a derecho event on 25 June 2008. In this case, surface observations were the only available tools which hinted at organized severe thunderstorm development just a couple of hours before the DMCS occurred.

By the mid-2010s onward, a few studies employing CAMs demonstrated limited potential for relatively greater success in simulating derecho events. The 1200 UTC 3 km WRF CAM simulations by Weisman et al. (2013) reasonably depicted the overall structure and severe wind potential of the 8 May 2009 DMCS across the central United States (as also done by Xu et al. 2015a,b). In addition, the 1200 UTC WRF run by Weisman et al. (2013) was also able to successfully simulate the observed unique warm-core-line-end vortex, with the WRF run initialized 24 h in advance of vortex development (Fig. 9). In Fierro et al. (2014), 3 km WRF simulations of the 29 June 2012 Ohio Valley DMCS showed better structural representation of the bow echo when regional radar data were assimilated into 6-h numerical forecasts (Figs. 21j–l). Assimilating lightning data into the 3 km WRF runs further improved the placement and timing of the DMCS (Figs. 21g–i), suggesting that better data assimilation techniques could appreciably improve short-term DMCS numerical forecasts. Numerous studies also

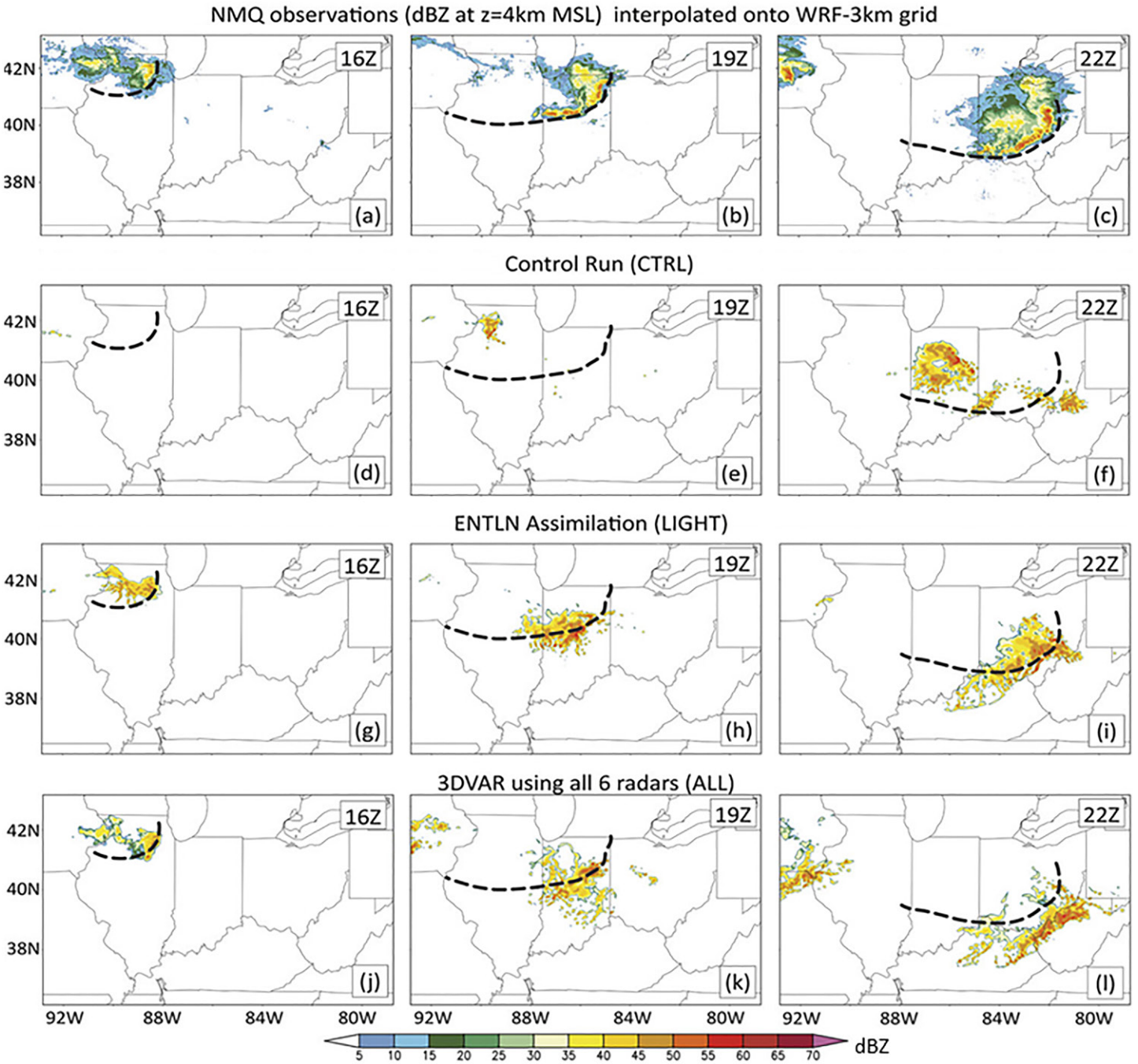

Fig. 21. Reflectivity fields (dBZ) at 4 km AGL. (a)–(c) Observed reflectivity; (d)–(f) control model run. (g)–(i) As in (d)–(f), but for run employing the lightning data assimilation. (j)–(l) As in (g)–(i), but for the 3DVAR assimilation incorporating radar data. Columns show data valid at (left) 1600, (center) 1900, and (right) 2200 UTC 29 Jun 2012. The thick black dashed curves denote the positions of the leading edge of the cold-pool boundary near the surface as inferred from clear-air NSSL mosaic reflectivity fields. [Adapted from Fierro et al. (2014, Fig. 5).]

reported great sensitivity in developing DMCSs when configuring CAMs with different initial and lateral boundary conditions, including some simulations not producing a DMCS at all (Toll et al. 2015; Grunzke and Evans 2017; Mathias et al. 2017, 2019). As a consequence of these findings, Ribeiro et al. (2022) simulated a DMCS (from 3 May 2020) with the 40-member convection-allowing Model for Prediction Across Scales (MPAS) ensemble, with individual members varying only initial conditions. Differences in ambient environments (i.e., dry biases in moisture profiles) or representation of convective initiation with varying initial conditions produced a wide range of solutions, with some members showing either no organized MCS, a highly organized bow echo, or a nonbowing MCS (Fig. 22), suggesting

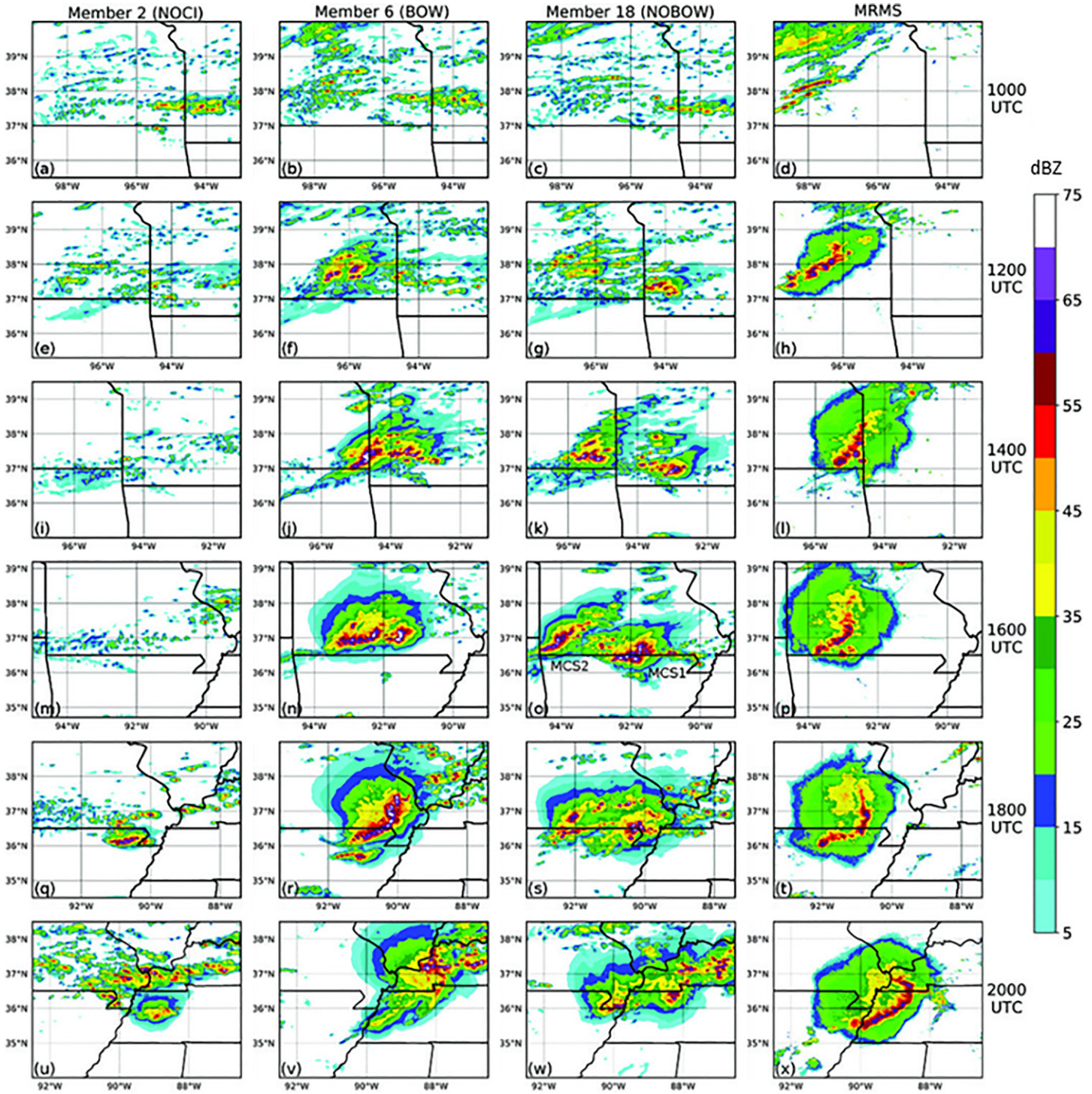

Fig. 22. Simulated composite reflectivity (dBZ) for members (first column) 2 (NOCI), (second column) 6 (BOW), and (third column) 18 (NOBOW) and (fourth column) MRMS composite reflectivity at (top to bottom) 1000, 1200, 1400, 1600, 1800, and 2000 UTC 3 May 2020, respectively. [Adapted from Ribeiro et al. (2022, Fig. 8).]

that improving initial conditions is just as important as improving model physics or data assimilation techniques to better forecast DMCSs in CAMs.

Dowell et al. (2022) showed that improvements made to the 3 km High-Resolution Rapid Refresh Model (HRRR; version 4) in 2020 resulted in fairly accurate simulations of the 10 August 2020 DMCS storm structure and accompanying severe wind swath across eastern Iowa into Illinois. However, these relatively successful deterministic CAM solutions were initialized well under 12 h in advance of derecho occurrence, providing little lead time for forecasters (Fig. 23). The HRRR is one of several CAMs employed in the

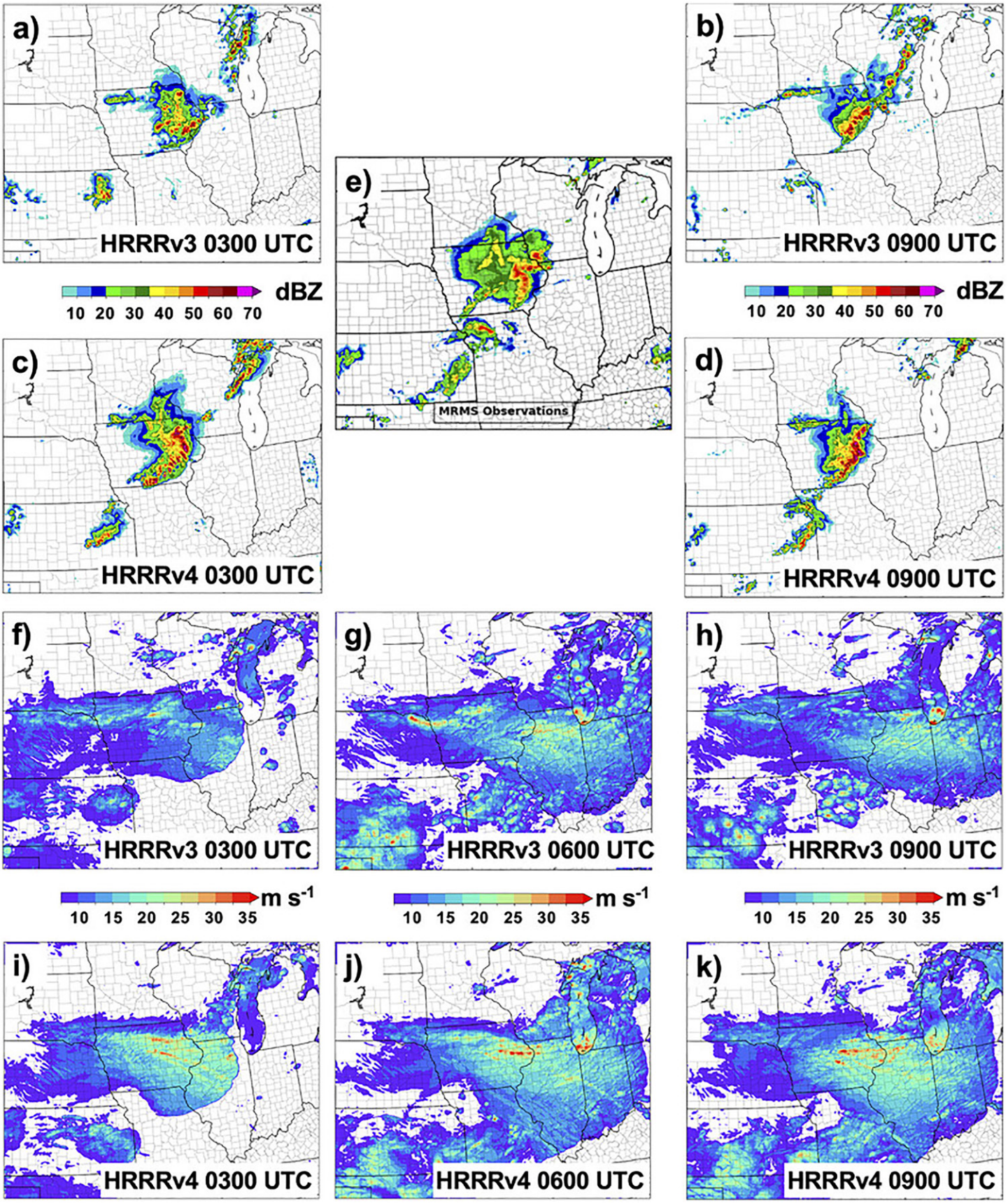

Fig. 23. (a),(b),(f),(g),(h) Operational HRRRv3 and (c),(d),(i),(j),(k) experimental HRRRv4 forecasts for the 10 Aug 2020 derecho. Composite radar reflectivity (dBZ) at 1800 UTC is shown for HRRR forecasts initialized at 0300 UTC in (a) and (c), HRRR forecasts initialized at 0900 UTC in (b) and (d), and MRMS observations in (e). Maximum 10 m wind speeds (m s^{-1}) during 0–18 h forecasts are shown for HRRR forecasts initialized at 0300 UTC in (f) and (i), 0600 UTC in (g) and (j), and 0900 UTC in (h) and (k). [From Dowell et al. (2022, Fig. 5).]

High-Resolution-Ensemble Forecast (HREF), many of which failed to simulate the parent DMCS for the 0000 UTC initialization (Gallus and Harrold 2023). Gallus and Harrold simulated the 10 August 2020 DMCS using the Finite-Volume-Cubed Sphere atmospheric dynamical core (FV3), initialized with HRRRv4, finding that the convection-allowing 3 km run failed to simulate the DMCS given preceding spurious convection contaminating the warm sector. However, when employing convective parameterization, their 3 km run reasonably simulated the derecho since downstream convection was suppressed and the environment remained pristine. While such a result may seem promising, convective parameterization is not often applied to 3-km-grid-spaced simulations, so questions remain regarding how downstream derecho environments should be parameterized in numerical guidance.

Multiple studies have shown improvements in the structural representation and damaging wind production of DMCSs when employing Δx finer than 3 km in real-case-based CAM simulations (Simon et al. 2011; Toll et al. 2015; Mathias et al. 2019; Shourd and Kaplan 2021). Weisman et al. (2013) hypothesized that leading-line mesovortices were poorly simulated in WRF runs of the 8 May 2009 DMCS because $\Delta x = 3$ km likely could not resolve the circulations. However, Xu et al. (2015a,b) showed that the leading-line mesovortices were better represented with 0.8 km Δx (Fig. 10). Similarly, Simon et al. (2011) successfully simulated the 40 m s^{-1} maximum wind gust observed with a DMCS when decreasing Δx from 2.8 to 1.5 km. Mathias et al. (2019) also found that the linear DMCS structures were better represented in 1 versus 3 km Δx runs of a cold-season derecho in western Europe, with Shourd and Kaplan (2021) producing similar results when simulating the 29 June 2012 warm-season progressive derecho with the WRF at 2 km Δx. Weisman et al. (2023) simulated multiple MCSs (some of which were DMCSs) with the WRF at 3 and 1 km Δx, finding that 1 km simulations better represented leading-line mesovortices (like Xu et al. 2015a,b), and potentially, the magnitude and expanse of the intense cold pools (compared to surface observations; Fig. 4). While changes in model configurations may not always influence whether a DMCS occurs in a CAM simulation, configuration changes may influence DMCS intensity and longevity, which is still crucial to understand so that further improvements to derecho numerical forecasts can be made.

Concluding remarks

Over the last several decades, strides have been made to better understand how derechos form and what features of a subset of MCSs support derecho development. Multiple studies have shown that MCSs, with a strong cold pool countered by just enough low-level shear to keep storm inflow from being undercut, with additional benefits of positive line-normal shear above the cold pool, are most likely to become long-lived enough to support derecho wind swaths. Furthermore, highly organized MCSs which can develop pronounced rear-inflow jets and mesovortices, both at the ends of convective lines and along the leading line of convection, are most likely to produce the most destructive wind gusts within derecho wind swaths. DMCSs can occur year-round in varying environments, ranging from classic tornado-outbreak patterns ahead of midlevel troughs or in subtly forced regimes associated with upper-ridge patterns. When it comes to forecasting derechos in the United States throughout the year, predicting derecho occurrence in warm-season synoptic environments that support the most intense DMCSs remains a challenge. Across the United States, summer DMCSs are often weakly forced and have proved difficult to forecast on a recurring basis including at short lead times. The one common denominator among warm-season derecho cases is that extreme instability and adequate vertical shear often coincide over a long corridor aligned with DMCS forward motion, allowing for a longer-lived and intense-wind-producing MCS than is seen in most other ambient environments. Still, even when overlapping extreme instability and adequate vertical shear overspread the Midwest and Ohio Valley in these long

corridors (where a summer derecho frequency climatological maximum exists), forecasting DMCS evolution in weakly forced environments remains problematic, limiting confidence in forecasts of derechos.

Some of the difficulties in forecasting weakly forced convection include determining when and where deep moist convection will initiate. For several MCSs (particularly at night), forecasting when elevated storms may become surface-based also remains a challenge, since the transition of MCSs from elevated to surface-based convection has recently been attributed to self-organizing processes associated with MCS cold-pool evolution (e.g., Miller et al. 2019; Parker et al. 2020; Parker 2021). As such, future research efforts in understanding and improving forecasts of convective evolution in weakly forced environments could be highly beneficial to operational forecasters.

Decreasing horizontal grid spacing down to around 3 km or less in CAM simulations has also significantly advanced derecho forecasting, and is necessary for realistically representing the storm-scale mechanisms and damaging wind potential associated with DMCSs. However, such results are contingent on developing a DMCS. Given the subtle forcing mechanisms that support intense warm-season derecho events, operational and research models still struggle to simulate warm-season progressive DMCSs in real-case based simulations. A commonality among most numerical DMCS studies is that model solutions were most sensitive to changes in the initial and lateral boundary conditions. Better forecasts of weakly forced convective events may continue to elude the meteorology community for several years to come. In the meantime, employing a convection-allowing ensemble with many members varying only initial conditions (as in Ribeiro et al. 2022) may provide an adequate spread in solutions needed for forecasters to assess the likelihood of a derecho occurrence when synoptic forcing is weak. As shown by some studies, numerical guidance for developing or ongoing DMCSs may improve further with the implementation of more sophisticated data assimilation techniques in CAMs, which in turn may improve placement, timing, and intensity details in near-term forecasts.

The Warn-on-Forecast System (WoFS) ensemble CAM framework (developed at the National Severe Storms Laboratory; Stensrud et al. 2009) has shown promise in improving forecasts of deep moist convection out to 12 h given its ability to ingest a vast amount of observations and employ sophisticated data assimilation techniques on a subhourly basis. By frequently assimilating radar data into individual runs, WoFs may improve on the structural representation of severe storms (Stensrud et al. 2013; Miller et al. 2022) in 6–12 h forecasts. Novel approaches to postprocessing of WoFs output, such as machine learning techniques, may also be used to extract meaningful signals from a plethora of complex severe weather scenarios to generate useful probabilistic guidance which could boost confidence in severe weather forecasts (Flora et al. 2021; Clark and Loken 2022). While MCSs have proved challenging for WoFs on a case-by-case basis (Stensrud et al. 2013), successful results were recently achieved with simulations of the 10 August 2020 derecho in several retroactive runs of WoFs on a larger spatial domain (Skinner et al. 2021). In these runs, WoFs consistently forecasted the DMCS across Iowa and Illinois with reasonable accuracy. Though WoFs could not resolve the highest observed surface wind speeds, ensemble members showed agreement in the occurrence of a near-hurricane-force surface wind swath associated with a passing MCS over eastern Iowa into Illinois. While earlier initialized WoFs runs demonstrated a northward displacement of the MCS and derecho wind swath, the derecho swath in simulations closer to observed MCS initiation time better overlapped with observations (Fig. 24). More retroactive WoFs simulations of warm-season progressive DMCSs with similar domain and model configurations to those employed for the 10 August 2020 should be performed to see if WoFs can routinely produce reliable progressive derecho forecasts, which would prove invaluable to forecasters.

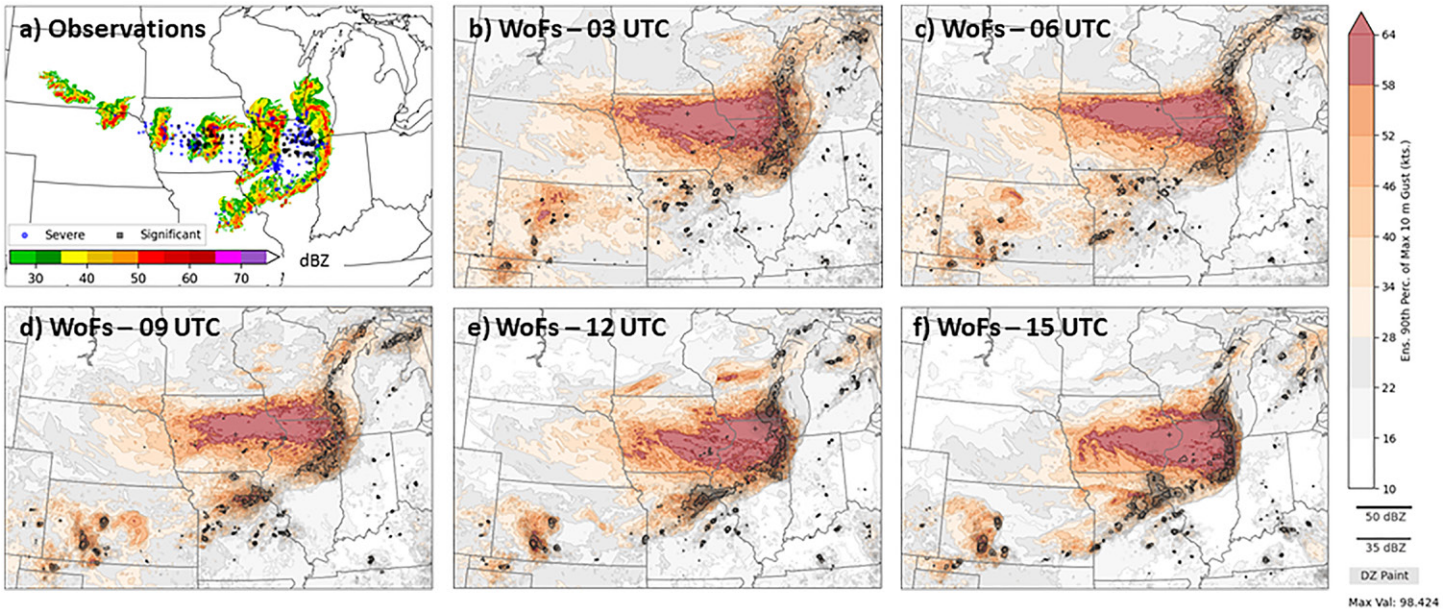

Fig. 24. (a) Composite reflectivity (dBZ) of the 10 Aug 2020 DMCS at 2.5 h intervals with reflectivity and gust reports ending at 2200 UTC. Gust reports for 50–65 kt magnitudes are shown as blue dots, with 65+ kt reports shown as black squares. WoFs output of the ensemble 90th-percentile accumulated maximum 10 m wind gusts (kt; shaded) are overlaid with 35 and 50 dBZ probability matched means (gray and black lined contours), initialized at (b) 0300, (c) 0600, (d) 0900, (e) 1200, and (f) 1500 UTC.

Acknowledgments. The authors thank the Editor Dr. Jeff Waldstreicher, Dr. Michael Coniglio, and two anonymous reviewers for the effort and time they have invested in providing detailed reviews, which contributed to a greatly improved manuscript.

Data availability statement. No datasets were generated with the current study. The only original figures were Figs. 13 and 20. In Fig. 13a, surface observations were retrieved from the Iowa Environmental Mesonet (IEM), available at https://mesonet.agron.iastate.edu/archive/, with the Surface Objective Analysis data archived internally at the Storm Prediction Center. The sounding in Fig. 13b was retrieved from the SPC event archive at https://www.spc.noaa.gov/exper/archive/event.php?date=20200810. Wind reports provided in Fig. 20 were retrieved from Storm Data, generated by the National Climatic Data Center, and are available for viewing via the Storm Prediction Center's Online Severe Plot (version 3.0) at https://www.spc.noaa.gov/climo/online/sp3/plot.php. Radar mosaics in Figs. 13a and 20a were also retrieved from the IEM and are available at https://mesonet.agron.iastate.edu/docs/nexrad_mosaic/. WoFs output in Figs. 20b–f were retrieved from https://wof.nssl.noaa.gov/realtime/?model=wofs&rd=20200810&rt=1500&product=ws_80_max&sector=wofs.

References

Alfaro, D. A., 2017: Low-tropospheric shear in the structure of squall lines: Impacts on latent heating under layer-lifting ascent. *J. Atmos. Sci.*, **74**, 229–248, https://doi.org/10.1175/JAS-D-16-0168.1.

Alfonso, A. P., and L. R. Naranjo, 1996: The 13 March 1993 severe squall line over western Cuba. *Wea. Forecasting*, **11**, 89–102, https://doi.org/10.1175/1520-0434(1996)011<0089:TMSSLO>2.0.CO;2.

Ashley, W. S., T. L. Mote, and M. L. Bentley, 2005: On the episodic nature of derecho-producing convective systems in the United States. *Int. J. Climatol.*, **25**, 1915–1932, https://doi.org/10.1002/joc.1229.

——, ——, and ——, 2007: An extensive episode of derecho-producing convective systems in the United States during May–June 1998: A multi-scale analysis and review. *Meteor. Appl.*, **14**, 227–244, https://doi.org/10.1002/met.23.

Atkins, N. T., and M. St. Laurent, 2009a: Bow echo mesovortices. Part I: Processes that influence their damaging potential. *Mon. Wea. Rev.*, **137**, 1497–1513, https://doi.org/10.1175/2008MWR2649.1.

——, and ——, 2009b: Bow echo mesovortices. Part II: Their genesis. *Mon. Wea. Rev.*, **137**, 1514–1532, https://doi.org/10.1175/2008MWR2650.1.

——, J. M. Arnott, R. W. Przybylinski, R. A. Wolf, and B. D. Ketcham, 2004: Vortex structure and evolution within bow echoes. Part I: Single-Doppler and damage analysis of the 29 June 1998 derecho. *Mon. Wea. Rev.*, **132**, 2224–2242, https://doi.org/10.1175/1520-0493(2004)132<2224:VSAEWB>2.0.CO;2.

——, C. S. Bouchard, R. W. Przybylinski, R. J. Trapp, and G. Schmocker, 2005: Damaging surface wind mechanism within the 10 June 2003 Saint Louis bow echo during BAMEX. *Mon. Wea. Rev.*, **133**, 2275–2296, https://doi.org/10.1175/MWR2973.1.

Bell, J. R., and Coauthors, 2022: Satellite-based characterization of convection and impacts from the catastrophic 10 August 2020 Midwest U.S. derecho. *Bull. Amer. Meteor. Soc.*, **103**, E1172–E1196, https://doi.org/10.1175/BAMS-D-21-0023.1.

Bentley, E. S., and J. Logsdon, 2016: An examination of the mesoscale environment and evolution of the northern Indiana/northwest Ohio derecho of 29 June 2012. *Electron. J. Severe Storms Meteor.*, **11** (1), https://ejssm.org/archives/wp-content/uploads/2021/09/vol11-1.pdf.

Bentley, M. L., and T. L. Mote, 2000: A synoptic climatology of cool-season derecho events. *Phys. Geogr.*, **21**, 21–37, https://doi.org/10.1080/02723646.2000.10642696.

——, and J. M. Sparks, 2003: A 15 yr climatology of derecho-producing mesoscale convective systems over the central and eastern United States. *Climate Res.*, **24**, 129–139, https://doi.org/10.3354/cr024129.

Bentley, M. A., T. L. Mote, and S. F. Byrd, 2000: A synoptic climatology of derecho producing mesoscale convective systems in the north-central plains. *Int. J. Climatol.*, **20**, 1329–1349, https://doi.org/10.1002/1097-0088(200009)20:11<1329::AID-JOC537>3.0.CO;2-F.

Bernardet, L. R., and W. R. Cotton, 1998: Multiscale evolution of a derecho-producing mesoscale convective system. *Mon. Wea. Rev.*, **126**, 2991–3015, https://doi.org/10.1175/1520-0493(1998)126<2991:MEOADP>2.0.CO;2.

Biggerstaff, M. I., and R. A. Houze Jr., 1991: Kinematic and precipitation structure of the 10–11 June 1985 squall line. *Mon. Wea. Rev.*, **119**, 3034–3065, https://doi.org/10.1175/1520-0493(1991)119<3034:KAPSOT>2.0.CO;2.

Braun, S. A., and R. A. Houze Jr., 1995: Melting and freezing in a mesoscale convective system. *Quart. J. Roy. Meteor. Soc.*, **121**, 55–77, https://doi.org/10.1002/qj.49712152104.

——, and ——, 1996: The heat budget of a midlatitude squall line and implications for potential vorticity production. *J. Atmos. Sci.*, **53**, 1217–1240, https://doi.org/10.1175/1520-0469(1996)053<1217:THBOAM>2.0.CO;2.

——, and ——, 1997: The evolution of the 10–11 June 1985 PRE-STORM squall line: Initiation, development of rear inflow, and dissipation. *Mon. Wea. Rev.*, **125**, 478–504, https://doi.org/10.1175/1520-0493(1997)125<0478:TEOTJP>2.0.CO;2.

Bryan, G. H., and R. Rotunno, 2008: Gravity currents in a deep anelastic atmosphere. *J. Atmos. Sci.*, **65**, 536–556, https://doi.org/10.1175/2007JAS2443.1.

——, and M. D. Parker, 2010: Observations of a squall line and its near environment using high-frequency rawinsonde launches during VORTEX2. *Mon. Wea. Rev.*, **138**, 4076–4097, https://doi.org/10.1175/2010MWR3359.1.

Burke, P. C., and D. M. Schultz, 2004: A 4-yr climatology of cold-season bow echoes over the continental United States. *Wea. Forecasting*, **19**, 1061–1074, https://doi.org/10.1175/811.1.

Campbell, M. A., A. E. Cohen, M. C. Coniglio, A. R. Dean, S. F. Corfidi, S. J. Corfidi, and C. M. Mead, 2017: Structure and motion of severe-wind-producing mesoscale convective systems and derechos in relation to the mean wind. *Wea. Forecasting*, **32**, 423–439, https://doi.org/10.1175/WAF-D-16-0060.1.

Celiński-Mysław, D., and D. Matuszko, 2014: An analysis of selected cases of derecho in Poland. *Atmos. Res.*, **149**, 263–281, https://doi.org/10.1016/j.atmosres.2014.06.016.

Charba, J., 1974: Application of gravity current model to analysis of squall-line gust front. *Mon. Wea. Rev.*, **102**, 140–156, https://doi.org/10.1175/1520-0493(1974)102<0140:AOGCMT>2.0.CO;2.

Chernokulsky, A., A. Shikhov, A. Bykov, N. Kalinin, M. Kurgansky, B. Sherstyukov, and Y. Yarinich, 2022: Diagnosis and modelling of two destructive derecho events in European Russia in the summer of 2010. *Atmos. Res.*, **267**, 105928, https://doi.org/10.1016/j.atmosres.2021.105928.

Clark, A. J., and E. D. Loken, 2022: Machine learning–derived severe weather probabilities from a Warn-on-Forecast system. *Wea. Forecasting*, **37**, 1721–1740, https://doi.org/10.1175/WAF-D-22-0056.1.

——, C. J. Schaffer, W. A. Gallus Jr., and K. Johnson-O'Mara, 2009: Climatology of storm reports relative to upper-level jet streaks. *Wea. Forecasting*, **24**, 1032–1051, https://doi.org/10.1175/2009WAF2222216.1.

Cohen, A. E., M. C. Coniglio, S. F. Corfidi, and S. J. Corfidi, 2007: Discrimination of mesoscale convective system environments using sounding observations. *Wea. Forecasting*, **22**, 1045–1062, https://doi.org/10.1175/WAF1040.1.

Coniglio, M. C., and D. J. Stensrud, 2001: Simulation of a progressive derecho using composite initial conditions. *Mon. Wea. Rev.*, **129**, 1593–1616, https://doi.org/10.1175/1520-0493(2001)129<1593:SOAPDU>2.0.CO;2.

——, and ——, 2004: Interpreting the climatology of derechos. *Wea. Forecasting*, **19**, 595–605, https://doi.org/10.1175/1520-0434(2004)019<0595:ITCOD>2.0.CO;2.

——, ——, and M. B. Richman, 2004: An observational study of derecho-producing convective systems. *Wea. Forecasting*, **19**, 320–337, https://doi.org/10.1175/1520-0434(2004)019<0320:AOSODC>2.0.CO;2.

——, ——, and L. J. Wicker, 2006: Effects of upper-level shear on the structure and maintenance of strong quasi-linear mesoscale convective systems. *J. Atmos. Sci.*, **63**, 1231–1252, https://doi.org/10.1175/JAS3681.1.

——, S. F. Corfidi, and J. S. Kain, 2011: Environment and early evolution of the 8 May 2009 derecho-producing convective system. *Mon. Wea. Rev.*, **139**, 1083–1102, https://doi.org/10.1175/2010MWR3413.1.

——, ——, and ——, 2012: Views on applying RKW theory: An illustration using the 8 May 2009 derecho-producing convective system. *Mon. Wea. Rev.*, **140**, 1023–1043, https://doi.org/10.1175/MWR-D-11-00026.1.

Corfidi, S. F., 2003: Cold pools and MCS propagation: Forecasting the motion of downwind-developing MCSs. *Wea. Forecasting*, **18**, 997–1017, https://doi.org/10.1175/1520-0434(2003)018<0997:CPAMPF>2.0.CO;2.

——, S. J. Corfidi, D. A. Imy, and A. L. Logan, 2006: A preliminary study of severe wind-producing MCSs in environments of limited moisture. *Wea. Forecasting*, **21**, 715–734, https://doi.org/10.1175/WAF947.1.

——, R. H. Johns, and M. A. Darrow, 2016: The Great Basin derecho of 31 May 1994. *Wea. Forecasting*, **31**, 917–935, https://doi.org/10.1175/WAF-D-15-0178.1.

Doswell, C. A., III, and J. S. Evans, 2003: Proximity sounding analysis for derechos and supercells: An assessment of similarities and differences. *Atmos. Res.*, **67–68**, 117–133, https://doi.org/10.1016/S0169-8095(03)00047-4.

Dowell, D. C., and Coauthors, 2022: The High-Resolution Rapid Refresh (HRRR): An hourly updating convection-allowing forecast model. Part I:

Motivation and system description. *Wea. Forecasting*, **37**, 1371–1395, https://doi.org/10.1175/WAF-D-21-0151.1.

Droegemeier, K. K., and R. B. Wilhelmson, 1987: Numerical simulation of thunderstorm outflow dynamics. Part I: Outflow sensitivity experiments and turbulence dynamics. *J. Atmos. Sci.*, **44**, 1180–1210, https://doi.org/10.1175/1520-0469(1987)044<1180:NSOTOD>2.0.CO;2.

Duke, J. W., and J. A. Rogash, 1992: Multiscale review of the development and early evolution of the 9 April 1991 derecho. *Wea. Forecasting*, **7**, 623–635, https://doi.org/10.1175/1520-0434(1992)007<0623:MROTDA>2.0.CO;2.

Dunn, J., and T. Best, 2011: Bow echo and mesovortex evolution during the 2 May 2007 North Texas derecho. *Electron. J. Severe Storms Meteor.*, **6** (4), https://ejssm.com/ojs/index.php/site/article/view/31/31.

Evans, C., M. L. Weisman, and L. F. Bosart, 2014: Development of an intense, warm-core mesoscale vortex associated with the 8 May 2009 "super derecho" convective event. *J. Atmos. Sci.*, **71**, 1218–1240, https://doi.org/10.1175/JAS-D-13-0167.1.

Evans, J. S., and C. A. Doswell III, 2001: Examination of derecho environments using proximity soundings. *Wea. Forecasting*, **16**, 329–342, https://doi.org/10.1175/1520-0434(2001)016<0329:EODEUP>2.0.CO;2.

Fierro, A. O., J. Gao, C. L. Ziegler, E. R. Mansell, D. R. MacGorman, and S. R. Dembek, 2014: Evaluation of a cloud-scale lightning data assimilation technique and a 3DVAR method for the analysis and short-term forecast of the 29 June 2012 derecho event. *Mon. Wea. Rev.*, **142**, 183–202, https://doi.org/10.1175/MWR-D-13-00142.1.

Flora, M. L., C. K. Potvin, P. S. Skinner, S. Handler, and A. McGovern, 2021: Using machine learning to generate storm-scale probabilistic guidance of severe weather hazards in the Warn-on-Forecast system. *Mon. Wea. Rev.*, **149**, 1535–1557, https://doi.org/10.1175/MWR-D-20-0194.1.

Flournoy, M. D., and M. C. Coniglio, 2019: Origins of vorticity in a simulated tornadic mesovortex observed during PECAN on 6 July 2015. *Mon. Wea. Rev.*, **147**, 107–134, https://doi.org/10.1175/MWR-D-18-0221.1.

Fovell, R. G., and Y. Ogura, 1989: Effect of vertical wind shear on numerically simulated multicell storm structure. *J. Atmos. Sci.*, **46**, 3144–3176, https://doi.org/10.1175/1520-0469(1989)046<3144:EOVWSO>2.0.CO;2.

——, and P. S. Dailey, 1995: The temporal behavior of numerically simulated multicell-type storms. Part I: Modes of behavior. *J. Atmos. Sci.*, **52**, 2073–2095, https://doi.org/10.1175/1520-0469(1995)052<2073:TTBONS>2.0.CO;2.

Fujita, T., 1955: Results of detailed synoptic studies of squall lines. *Tellus*, **7**, 405–436, https://doi.org/10.3402/tellusa.v7i4.8920.

——, 1959: Precipitation and cold air production in mesoscale thunderstorm systems. *J. Meteor.*, **16**, 454–466, https://doi.org/10.1175/1520-0469(1959)016<0454:PACAPI>2.0.CO;2.

Fujita, T. T., 1978: Manual of downburst identification for project NIMROD. Satellite and Mesometeorology Research Paper 156, 104 pp., https://ntrs.nasa.gov/citations/19780022828.

Gallus, W. A., Jr., and R. H. Johnson, 1995a: The dynamics of circulations within the trailing stratiform region of squall lines. Part I: The 10–11 June PRE-STORM system. *J. Atmos. Sci.*, **52**, 2161–2187, https://doi.org/10.1175/1520-0469(1995)052<2161:TDOCWT>2.0.CO;2.

——, and ——, 1995b: The dynamics of circulations within the trailing stratiform regions of squall lines. Part II: Influence of the convective line and ambient environment. *J. Atmos. Sci.*, **52**, 2188–2211, https://doi.org/10.1175/1520-0469(1995)052<2188:TDOCWT>2.0.CO;2.

——, and A. C. Duhachek, 2022: Differences in near-storm parameters useful for forecasting intensity of nocturnal and diurnal bow echo winds. *Wea. Forecasting*, **37**, 2331–2347, https://doi.org/10.1175/WAF-D-21-0213.1.

——, and M. A. Harrold, 2023: Challenges in numerical weather prediction of the 10 August 2020 midwestern derecho: Examples from the FV3-LAM. *Wea. Forecasting*, **38**, 1429–1445, https://doi.org/10.1175/WAF-D-23-0019.1.

——, J. C. Correia, and I. Jankov, 2005: The 4 June 1999 derecho event: A particularly difficult challenge for numerical weather prediction. *Wea. Forecasting*, **20**, 705–728, https://doi.org/10.1175/WAF883.1.

Garner, S. T., and A. J. Thorpe, 1992: The development of organized convection in a simplified squall-line model. *Quart. J. Roy. Meteor. Soc.*, **118**, 101–124, https://doi.org/10.1002/qj.49711850306.

Gatzen, C., 2004: A derecho in Europe: Berlin, 10 July 2002. *Wea. Forecasting*, **19**, 639–645, https://doi.org/10.1175/1520-0434(2004)019<0639:ADIEBJ>2.0.CO;2.

——, A. H. Fink, D. M. Schultz, and J. G. Pinto, 2020: An 18-year climatology of derechos in Germany. *Nat. Hazards Earth Syst. Sci.*, **20**, 1335–1351, https://doi.org/10.5194/nhess-20-1335-2020.

Grim, J. A., R. M. Rauber, G. M. McFarquhar, B. F. Jewett, and D. P. Jorgensen, 2009: Development and forcing of the rear inflow jet in a rapidly developing and decaying squall line during BAMEX. *Mon. Wea. Rev.*, **137**, 1206–1229, https://doi.org/10.1175/2008MWR2503.1.

Grunzke, C. T., and C. Evans, 2017: Predictability and dynamics of warm-core mesoscale vortex formation with the 8 May 2009 "Super Derecho" event. *Mon. Wea. Rev.*, **145**, 811–832, https://doi.org/10.1175/MWR-D-16-0217.1.

Guastini, C. T., and L. F. Bosart, 2016: Analysis of a progressive derecho climatology and associated formation environments. *Mon. Wea. Rev.*, **144**, 1363–1382, https://doi.org/10.1175/MWR-D-15-0256.1.

Hamid, K., 2012: Investigation of the passage of a derecho in Belgium. *Atmos. Res.*, **107**, 86–105, https://doi.org/10.1016/j.atmosres.2011.12.013.

Hamilton, R. A., J. W. Archbold, and C. K. M. Douglas, 1945: Meteorology of Nigeria and adjacent territory. *Quart. J. Roy. Meteor. Soc.*, **71**, 231–264, https://doi.org/10.1002/qj.49707130905.

Houze, R. A., 2018: 100 years of research on mesoscale convective systems. *A Century of Progress in Atmospheric and Related Sciences: Celebrating the American Meteorological Society Centennial*, *Meteor. Monogr.*, No. 59, Amer. Meteor. Soc., https://doi.org/10.1175/AMSMONOGRAPHS-D-18-0001.1.

Houze, R. A., Jr., S. A. Rutledge, M. I. Biggerstaff, and B. F. Smull, 1989: Interpretation of Doppler weather radar displays in midlatitude mesoscale convective systems. *Bull. Amer. Meteor. Soc.*, **70**, 608–619, https://doi.org/10.1175/1520-0477(1989)070<0608:IODWRD>2.0.CO;2.

James, R. P., P. M. Markowski, and J. M. Fritsch, 2006: Bow echo sensitivity to ambient moisture and cold pool strength. *Mon. Wea. Rev.*, **134**, 950–964, https://doi.org/10.1175/MWR3109.1.

Johns, R. H., 1982: A synoptic climatology of northwest-flow severe weather outbreaks. Part I: Nature and significance. *Mon. Wea. Rev.*, **110**, 1653–1663, https://doi.org/10.1175/1520-0493(1982)110<1653:ASCONF>2.0.CO;2.

——, 1984: A synoptic climatology of northwest-flow severe weather outbreaks. Part II: Meteorological parameters and synoptic patterns. *Mon. Wea. Rev.*, **112**, 449–464, https://doi.org/10.1175/1520-0493(1984)112<0449:ASCONF>2.0.CO;2.

——, 1993: Meteorological conditions associated with bow echo development in convective storms. *Wea. Forecasting*, **8**, 294–299, https://doi.org/10.1175/1520-0434(1993)008<0294:MCAWBE>2.0.CO;2.

——, and W. D. Hirt, 1987: Derechos: Widespread convectively induced windstorms. *Wea. Forecasting*, **2**, 32–49, https://doi.org/10.1175/1520-0434(1987)002<0032:DWCIW>2.0.CO;2.

Kleyla, R. P., and R. E. Peterson, 1990: A case study of a derecho (windstorm) in the central plains. *J. Wind Eng. Ind. Aerodyn.*, **36**, 87–96, https://doi.org/10.1016/0167-6105(90)90295-N.

Klimowski, B. A., M. R. Hjelmfelt, and M. J. Bunkers, 2004: Radar observations of the early evolution of bow echoes. *Wea. Forecasting*, **19**, 727–734, https://doi.org/10.1175/1520-0434(2004)019<0727:ROOTEE>2.0.CO;2.

Lafore, J.-P., and M. W. Moncrieff, 1989: A numerical investigation of the organization and interaction of the convective and stratiform regions of tropical squall lines. *J. Atmos. Sci.*, **46**, 521–544, https://doi.org/10.1175/1520-0469(1989)046<0521:ANIOTO>2.0.CO;2.

López, J. M., 2007: A Mediterranean derecho: Catalonia (Spain), 17th August 2003. *Atmos. Res.*, **83**, 272–283, https://doi.org/10.1016/j.atmosres.2005.08.008.

Lyza, A. W., A. W. Clayton, K. R. Knupp, E. Lenning, M. T. Friedlein, R. Castro, and E. S. Bentley, 2017: Analysis of mesovortex characteristics, behavior, and

interactions during the second 30 June–1 July 2014 midwestern derecho event. *Electron. J. Severe Storms Meteor.*, **12** (2), https://ejssm.com/ojs/index.php/site/article/view/67/66.

Mahoney, K. M., and G. M. Lackmann, 2011: The sensitivity of momentum transport and severe surface winds to environmental moisture in idealized simulations of a mesoscale convective system. *Mon. Wea. Rev.*, **139**, 1352–1369, https://doi.org/10.1175/2010MWR3468.1.

Mathias, L., V. Ermert, F. D. Kelemen, P. Ludwig, and J. G. Pinto, 2017: Synoptic analysis and hindcast of an intense bow echo in western Europe: The 9 June 2014 storm. *Wea. Forecasting*, **32**, 1121–1141, https://doi.org/10.1175/WAF-D-16-0192.1.

——, P. Ludwig, and J. G. Pinto, 2019: Synoptic-scale conditions and convection-resolving hindcast experiments of a cold-season derecho on 3 January 2014 in western Europe. *Nat. Hazards Earth Syst. Sci.*, **19**, 1023–1040, https://doi.org/10.5194/nhess-19-1023-2019.

Mauri, E. L., and W. A. Gallus Jr., 2021: Differences between severe and nonsevere warm-season, nocturnal bow echo environments. *Wea. Forecasting*, **36**, 53–74, https://doi.org/10.1175/WAF-D-20-0137.1.

McFarquhar, G. M., M. S. Timlin, R. M. Rauber, B. F. Jewett, J. A. Grim, and D. P. Jorgensen, 2007: Vertical variability of cloud hydrometeors in the stratiform region of mesoscale convective systems and bow echoes. *Mon. Wea. Rev.*, **135**, 3405–3428, https://doi.org/10.1175/MWR3444.1.

Metz, N. D., and L. F. Bosart, 2010: Derecho and MCS development, evolution, and multiscale interactions during 3–5 July 2003. *Mon. Wea. Rev.*, **138**, 3048–3070, https://doi.org/10.1175/2010MWR3218.1.

Miller, R. L., C. L. Ziegler, and M. I. Biggerstaff, 2019: Seven-Doppler radar and in situ analysis of the 25–26 June 2015 Kansas MCS during PECAN. *Mon. Wea. Rev.*, **148**, 211–240, https://doi.org/10.1175/MWR-D-19-0151.1.

Miller, W. J., and Coauthors, 2022: Exploring the usefulness of downscaling free forecasts from the Warn-on-Forecast system. *Wea. Forecasting*, **37**, 181–203, https://doi.org/10.1175/WAF-D-21-0079.1.

Moller, A. R., C. A. Doswell, M. P. Foster, and G. R. Woodall, 1994: The operational recognition of supercell thunderstorm environments and storm structures. *Wea. Forecasting*, **9**, 327–347, https://doi.org/10.1175/1520-0434(1994)009<0327:TOROST>2.0.CO;2.

Mulholland, J. P., J. M. Peters, and H. Morrison, 2021: How does vertical wind shear influence entrainment in squall lines? *J. Atmos. Sci.*, **78**, 1931–1946, https://doi.org/10.1175/JAS-D-20-0299.1.

Newton, C. W., 1950: Structure and mechanisms of the prefrontal squall line. *J. Meteor.*, **7**, 210–222, https://doi.org/10.1175/1520-0469(1950)007<0210:SAMOTP>2.0.CO;2.

Ogura, Y., and Y. Chen, 1977: A life history of an intense mesoscale convective storm in Oklahoma. *J. Atmos. Sci.*, **34**, 1458–1476, https://doi.org/10.1175/1520-0469(1977)034<1458:ALHOAI>2.0.CO;2.

Pandya, R. E., D. R. Durran, and M. L. Weisman, 2000: The influence of convective thermal forcing on the three-dimensional circulation around squall lines. *J. Atmos. Sci.*, **57**, 29–45, https://doi.org/10.1175/1520-0469(2000)057<0029:TIOCTF>2.0.CO;2.

Parker, M. D., 2021: Self-organization and maintenance of simulated nocturnal convective systems from PECAN. *Mon. Wea. Rev.*, **149**, 999–1022, https://doi.org/10.1175/MWR-D-20-0263.1.

——, and R. H. Johnson, 2004: Structures and dynamics of quasi-2D mesoscale convective systems. *J. Atmos. Sci.*, **61**, 545–567, https://doi.org/10.1175/1520-0469(2004)061<0545:SADOQM>2.0.CO;2.

——, B. S. Borchardt, R. L. Miller, and C. L. Ziegler, 2020: Simulated evolution and severe wind production by the 25–26 June 2015 nocturnal MCS from PECAN. *Mon. Wea. Rev.*, **148**, 183–209, https://doi.org/10.1175/MWR-D-19-0072.1.

Peters, K., and C. Hohenegger, 2017: On the dependence of squall-line characteristics on surface conditions. *J. Atmos. Sci.*, **74**, 2211–2228, https://doi.org/10.1175/JAS-D-16-0290.1.

Price, C. G., and B. P. Murphy, 2002: Lightning activity during the 1999 Superior derecho. *Geophys. Res. Lett.*, **29**, 2142, https://doi.org/10.1029/2002GL015488.

Przybylinski, R. W., 1995: The bow echo: Observations, numerical simulations, and severe weather detection methods. *Wea. Forecasting*, **10**, 203–218, https://doi.org/10.1175/1520-0434(1995)010<0203:TBEONS>2.0.CO;2.

Púčik, T., M. Francová, D. Rýva, M. Kolář, and L. Ronge, 2011: Forecasting challenges during the severe weather outbreak in central Europe on 25 June 2008. *Atmos. Res.*, **100**, 680–704, https://doi.org/10.1016/j.atmosres.2010.11.014.

Punkka, A.-J., J. Teittinen, and R. H. Johns, 2006: Synoptic and mesoscale analysis of a high-latitude derecho-severe thunderstorm outbreak in Finland on 5 July 2002. *Wea. Forecasting*, **21**, 752–763, https://doi.org/10.1175/WAF953.1.

Ribeiro, B. Z., S. J. Weiss, and L. F. Bosart, 2022: An analysis of the 3 May 2020 low-predictability derecho using a convection-allowing MPAS ensemble. *Wea. Forecasting*, **37**, 219–239, https://doi.org/10.1175/WAF-D-21-0092.1.

Rutledge, S. A., and R. A. Houze Jr., 1987: A diagnostic modeling study of the trailing stratiform region of a midlatitude squall line. *J. Atmos. Sci.*, **44**, 2640–2656, https://doi.org/10.1175/1520-0469(1987)044<2640:ADMSOT>2.0.CO;2.

Scott, J. D., and S. A. Rutledge, 1995: Doppler radar observations of an asymmetric mesoscale convective system and associated vortex couplet. *Mon. Wea. Rev.*, **123**, 3437–3457, https://doi.org/10.1175/1520-0493(1995)123<3437:DROOAA>2.0.CO;2.

Shourd, K. S., and M. L. Kaplan, 2021: The multiscale dynamics of the 29 June 2012 super derecho. *Climate*, **9**, 155, https://doi.org/10.3390/cli9110155.

Simon, A., J. Kaňák, A. Sokol, M. Putsay, L. Uhrínová, K. Csirmaz, L. Okon, and R. Habrovský, 2011: Case study of a severe windstorm over Slovakia and Hungary on 25 June 2008. *Atmos. Res.*, **100**, 705–739, https://doi.org/10.1016/j.atmosres.2010.12.012.

Sipos, Z., A. Simon, K. Csirmaz, T. Lemler, R.-D. Manta, and Z. Kocsis, 2021: A case study of a derecho storm in a dry, high-shear environment. *Quart. J. Hung. Meteor. Serv.*, **125** (1), 1–37, https://doi.org/10.28974/idojaras.2021.1.1.

Skinner, P., and Coauthors, 2021: Predictability of the 10 August 2020 Midwest derecho. *Major Weather Events and Impacts of 2020*, Online, Amer. Meteor. Soc., 13.5, https://ams.confex.com/ams/101ANNUAL/meetingapp.cgi/Paper/386391.

Squitieri, B. J., A. R. Wade, and I. L. Jirak, 2023: A historical overview on the science of derechos. Part I: Identification, climatology, and societal impacts. *Bull. Amer. Meteor. Soc.*, https://doi.org/10.1175/BAMS-D-22-0217.1, in press.

Stensrud, D. J., and Coauthors, 2009: Convective-scale Warn-on-Forecast system: A vision for 2020. *Bull. Amer. Meteor. Soc.*, **90**, 1487–1500, https://doi.org/10.1175/2009BAMS2795.1.

——, and Coauthors, 2013: Progress and challenges with warn-on-forecast. *Atmos. Res.*, **123**, 2–16, https://doi.org/10.1016/j.atmosres.2012.04.004.

Sun, J., S. Braun, M. I. Biggerstaff, R. G. Fovell, and R. A. Houze Jr., 1993: Warm upper-level downdrafts associated with a squall line. *Mon. Wea. Rev.*, **121**, 2919–2927, https://doi.org/10.1175/1520-0493(1993)121<2919:WULDAW>2.0.CO;2.

Surowiecki, A., and M. Taszarek, 2020: A 10-year radar-based climatology of mesoscale convective system archetypes and derechos in Poland. *Mon. Wea. Rev.*, **148**, 3471–3488, https://doi.org/10.1175/MWR-D-19-0412.1.

Szeto, J. M., and H. Cho, 1994: A numerical investigation of squall lines. Part II: The mechanics of evolution. *J. Atmos. Sci.*, **51**, 425–433, https://doi.org/10.1175/1520-0469(1994)051<0425:ANIOSL>2.0.CO;2.

Takemi, T., 1999: Structure and evolution of a severe squall line over the arid region in northwest China. *Mon. Wea. Rev.*, **127**, 1301–1309, https://doi.org/10.1175/1520-0493(1999)127<1301:SAEOAS>2.0.CO;2.

Tao, W.-K., J. R. Scala, B. Ferrier, and J. Simpson, 1995: The effect of melting processes on the development of a tropical and midlatitude squall line. *J. Atmos. Sci.*, **52**, 1934–1948, https://doi.org/10.1175/1520-0469(1995)052<1934:TEOMPO>2.0.CO;2.

Taszarek, M., and Coauthors, 2019: Derecho evolving from a mesocyclone—A study of 11 August 2017 severe weather outbreak in Poland: Event analysis and high-resolution simulation. *Mon. Wea. Rev.*, **147**, 2283–2306, https://doi.org/10.1175/MWR-D-18-0330.1.

Tepper, M., 1950: A proposed mechanism of squall lines: The pressure jump line. *J. Meteor.*, **7**, 21–29, https://doi.org/10.1175/1520-0469(1950)007<0021:APMOSL>2.0.CO;2.

Toll, V., A. Männik, A. Luhmaa, and R. Rõõm, 2015: Hindcast experiments of the derecho in Estonia on 08 August, 2010: Modeling derecho with NWP model HARMONIE. *Atmos. Res.*, **158–159**, 179–191, https://doi.org/10.1016/j.atmosres.2014.10.011.

Trapp, R. J., and M. L. Weisman, 2003: Low-level mesovortices within squall lines and bow echoes. Part II: Their genesis and implications. *Mon. Wea. Rev.*, **131**, 2804–2823, https://doi.org/10.1175/1520-0493(2003)131<2804:LMWSLA>2.0.CO;2.

Uccellini, L. W., and D. R. Johnson, 1979: The coupling of upper and lower tropospheric jet streaks and implications for the development of severe convective storms. *Mon. Wea. Rev.*, **107**, 682–703, https://doi.org/10.1175/1520-0493(1979)107<0682:TCOUAL>2.0.CO;2.

Wakimoto, R. M., 1985: Forecasting dry microburst activity over the high plains. *Mon. Wea. Rev.*, **113**, 1131–1143, https://doi.org/10.1175/1520-0493(1985)113<1131:FDMAOT>2.0.CO;2.

——, H. V. Murphey, A. Nester, D. P. Jorgensen, and N. T. Atkins, 2006a: High winds generated by bow echoes. Part I: Overview of the Omaha bow echo 5 July 2003 storm during BAMEX. *Mon. Wea. Rev.*, **134**, 2793–2812, https://doi.org/10.1175/MWR3215.1.

——, ——, C. A. Davis, and N. T. Atkins, 2006b: High winds generated by bow echoes. Part II: The relationship between the mesovortices and damaging straight-line winds. *Mon. Wea. Rev.*, **134**, 2813–2829, https://doi.org/10.1175/MWR3216.1.

Weisman, M. L., 1992: The role of convectively generated rear-inflow jets in the evolution of long-lived mesoconvective systems. *J. Atmos. Sci.*, **49**, 1826–1847, https://doi.org/10.1175/1520-0469(1992)049<1826:TROCGR>2.0.CO;2.

——, 1993: The genesis of severe, long lived bow echoes. *J. Atmos. Sci.*, **50**, 645–670, https://doi.org/10.1175/1520-0469(1993)050<0645:TGOSLL>2.0.CO;2.

——, 2001: Bow echoes: A tribute to T. T. Fujita. *Bull. Amer. Meteor. Soc.*, **82**, 97–116, https://doi.org/10.1175/1520-0477(2001)082<0097:BEATTT>2.3.CO;2.

——, and C. A. Davis, 1998: Mechanisms for the generation of mesoscale vortices within quasi-linear convective systems. *J. Atmos. Sci.*, **55**, 2603–2622, https://doi.org/10.1175/1520-0469(1998)055<2603:MFTGOM>2.0.CO;2.

——, and R. J. Trapp, 2003: Low-level mesovortices within squall lines and bow echoes. Part I: Overview and dependence on environmental shear. *Mon. Wea. Rev.*, **131**, 2779–2803, https://doi.org/10.1175/1520-0493(2003)131<2779:LMWSLA>2.0.CO;2.

——, and R. Rotunno, 2004: "A theory for strong long-lived squall lines" revisited. *J. Atmos. Sci.*, **61**, 361–382, https://doi.org/10.1175/1520-0469(2004)061<0361:ATFSLS>2.0.CO;2.

——, C. Evans, and I. Bosart, 2013: The 8 May 2009 superderecho: Analysis of a real-time explicit convective forecast. *Wea. Forecasting*, **28**, 863–892, https://doi.org/10.1175/WAF-D-12-00023.1.

——, K. Manning, R. Sobash, and C. Schwartz, 2023: Simulations of severe convective systems using 1-versus 3-km grid spacing. *Wea. Forecasting*, **38**, 401–423, https://doi.org/10.1175/WAF-D-22-0112.1.

Wheatley, D. M., and R. J. Trapp, 2008: The effect of mesoscale heterogeneity on the genesis and structure of mesovortices within quasi-linear convective systems. *Mon. Wea. Rev.*, **136**, 4220–4241, https://doi.org/10.1175/2008MWR2294.1.

——, ——, and N. T. Atkins, 2006: Radar and damage analysis of severe bow echoes observed during BAMEX. *Mon. Wea. Rev.*, **134**, 791–806, https://doi.org/10.1175/MWR3100.1.

Wilhelmson, R. B., and C.-S. Chen, 1982: A simulation of the development of successive cells along a cold outflow boundary. *J. Atmos. Sci.*, **39**, 1466–1483, https://doi.org/10.1175/1520-0469(1982)039<1466:ASOTDO>2.0.CO;2.

Xu, X., M. Xue, and Y. Wang, 2015a: Mesovortices within the 8 May 2009 bow echo over the central United States: Analyses of the characteristics and evolution based on Doppler radar observations and a high-resolution model simulation. *Mon. Wea. Rev.*, **143**, 2266–2290, https://doi.org/10.1175/MWR-D-14-00234.1.

——, ——, and ——, 2015b: The genesis of mesovortices within a real-data simulation of a bow echo system. *J. Atmos. Sci.*, **72**, 1963–1986, https://doi.org/10.1175/JAS-D-14-0209.1.

Xue, M., 2002: Density currents in shear flows: Effects of rigid lid and cold-pool internal circulation, and application to squall line dynamics. *Quart. J. Roy. Meteor. Soc.*, **128**, 47–73, https://doi.org/10.1256/00359000260498789.

Yang, M.-H., and R. A. Houze Jr., 1995: Sensitivity of squall-line rear inflow to ice microphysics and environmental humidity. *Mon. Wea. Rev.*, **123**, 3175–3193, https://doi.org/10.1175/1520-0493(1995)123<3175:SOSLRI>2.0.CO;2.

Yang, M.-J., and R. A. Houze Jr., 1996: Momentum budget of a squall line with trailing stratiform precipitation: Calculations with a high-resolution numerical model. *J. Atmos. Sci.*, **53**, 3629–3652, https://doi.org/10.1175/1520-0469(1996)053<3629:MBOASL>2.0.CO;2.

Zhang, D.-L., and K. Gao, 1989: Numerical simulation of an intense squall line during 10–11 June 1985 PRE-STORM. Part II: Rear inflow, surface pressure perturbations and stratiform precipitation. *Mon. Wea. Rev.*, **117**, 2067–2094, https://doi.org/10.1175/1520-0493(1989)117<2067:NSOAIS>2.0.CO;2.

——, and H.-R. Cho, 1992: The development of negative moist potential vorticity in the stratiform region of a simulated squall line. *Mon. Wea. Rev.*, **120**, 1322–1341, https://doi.org/10.1175/1520-0493(1992)120<1322:TDONMP>2.0.CO;2.